CDF/ANAL/EXOTIC/CDFR/10496
Version 2.0
May 6, 2011

Search for Anomalous Production of Events with a W or Z Boson and Additional Leptons

S. Wilbur, D. Krop, C. Grosso-Pilcher, H. Frisch
University of Chicago

Abstract

We present a search for anomalous production of events containing a W or Z boson and additional leptons. The search uses data corresponding to 5.1 fb^{-1} of integrated luminosity from $p\bar{p}$ collisions at a center-of-mass energy of $\sqrt{s} = 1.96$ TeV. We find no indications of non-standard-model phenomena. Limits are set for a dark-matter inspired model of supersymmetric dark sector Higgs production.

Contents

1 Introduction

In the standard model (SM) of particle physics, the mass of the Higgs boson is constrained to be larger than 114.4 GeV by the LEP experiments [1]. If the Higgs has evaded detection via non-standard decays, however, this limit can be avoided. There are various proposals for such a *hidden* Higgs sector in the literature in the context of the NMSSM [2], little Higgs models [3], R-parity violating MSSM [4], and others. One of the recent promising proposals involves the phenomenology of light supersymmetric hidden sectors [5] where the lightest visible superpartner, the equivalent of the LSP in the MSSM, is allowed to cascade into a hidden sector. The existence of such sectors has been further motivated by recent observed astrophysical anomalies [6] which may be signatures of dark matter annihilations [7] or decays into a light hidden sector [8]. Ref. [9] presents a model of Higgs decay to a light hidden sector resulting in events with a high multiplicity of leptons. Due to this high multiplicity the momenta of the leptons would tend to be low, predominantly below 20 GeV, and these events would not have been previously identified.

In this paper we present a search for the anomalous production of W and Z bosons in association with additional leptons with p_T down to 3 GeV for muons and 1 GeV for electrons. We present our results as a limit on a model that is representative of these theories, described in Ref. [9].

2 Analysis Strategy

The analysis uses the W and Z samples, selected via the high-p_T electron and muon triggers. These samples are well understood, but we still validate the selections by calculating the R ratio, $R = \sigma(W)/\sigma(Z)$, and comparing it to NNLO predictions. We then develop specialized tools to identify low-p_T electrons and muons. We use these tools in addition to standard high-p_T lepton identification to obtain the W/Z + lepton multiplicity distributions. The Monte Carlo reproduces global features of W and Z events well, but does not accurately model the efficiency or fake rate of soft lepton identification. Therefore, we parameterize the response of the soft lepton identification based on kinematic variables, and then normalize the results to the number of data events with exactly one additional lepton. Finally, we compare the multiplicity distributions of additional leptons in W/Z events to the standard model prediction.

3 Datasets

The analysis uses events selected with the triggers "`ELECTRON_CENTRAL_18`", "`MUON_CMUP18`", and "`MUON_CMX18`". We use good run list "`goodrun_v37_em_mu_si.list`" requiring good electrons, muons, and silicon. The datasets, runs, run periods, and luminosities are listed in Table 1. The data encompass CDF Periods 1 to 27, covering the calendar period Dec. 7, 2004 to Jan. 6, 2010. The total luminosity for this dataset is 5.1 fb^{-1}, and the numbers of electron- and muon-triggered events are 384,622,495 and 224,359,512, respectively.

The main backgrounds are W + jets, Drell-Yan, $Z \to \tau\tau$, $t\bar{t}$, single top, and diboson production. We have modeled these using the Alpgen [10] or Pythia [11] Monte Carlo

Dataset	Period	Runs	Luminosity	Dates
0h	1	190697 – 195408	363pb^{-1}	7 Dec 04 - 18 Mar 05
	2	195409 – 198379		19 Mar 05 - 20 May 05
	3	198380 – 201349		21 May 05 - 19 Jul 05
	4	201350 – 203799		20 Jul 05 - 4 Sep 05
0i	5	203819 – 206989	587pb^{-1}	5 Sep 05 - 9 Nov 05
	6	206990 – 210011		10 Nov 05 - 14 Jan 06
	7	210012 – 212133		14 Jan 06 - 22 Feb 06
	8	217990 – 222426		9 Jun 06 - 1 Sep 06
	9	222529 – 228596		1 Sep 06 - 22 Nov 06
0j	10	228664 – 233111	945pb^{-1}	24 Nov 06 - 30 Jan 07
	11	233133 – 237795		30 Jan 07 - 31 Mar 07
	12	237845 – 241664		1 Apr 07 - 13 May 07
	13	241665 – 246231		13 May 07 - 4 Aug 07
0k	14	252836 – 254686	484pb^{-1}	28 Oct 07 - 3 Dec 07
	15	254800 – 256824		5 Dec 07 - 27 Jan 08
	16	256840 – 258787		27 Jan 08 - 27 Feb 08
	17	258880 – 261005		28 Feb 08 - 16 Apr 08
0m	18	261119 – 264071	2687pb^{-1}	18 Apr 08 - 1 Jul 08
	19	264101 – 266513		1 Jul 08 - 24 Aug 08
	20	266528 – 267718		24 Aug 08 - 4 Oct 08
	21	268155 – 271047		12 Oct 08 - 1 Jan 09
	22	271072 – 272214		2 Jan 09 - 10 Feb 09
	23	272470 – 274055		15 Feb 09 - 21 Mar 09
	24	274123 – 275848		22 Mar 09 - 4 May 09
	25	275873 – 277511		5 May 09 - 13 Jun 09
	26	282976 – 284843		15 Sep 09 - 25 Oct 09
	27	284858 – 287261		25 Nov 09 - 06 Jan 10

Table 1: Datasets used in the analysis. Both muon and electron datasets are used, i.e. $0h$ refers to bhmubh and bhelbh. The luminosities of the electron and muon datasets are the same because we use unprescaled triggers and the same good run list for both triggers.

Tight Central Electron Cuts
$\eta_{\text{Detector}} \leq 1.1$
Track must be fiducial to CES
$E_T \geq 20$ GeV
$E_{HAD}/E_{EM} \leq 0.055 + 0.00045 \times E$
$\text{Iso}(R = 0.4)/E_T \leq 0.1$
$p_T \geq 10$ GeV
≥ 3 COT axial segments with ≥ 5 hits
≥ 2 COT stereo segments with ≥ 5 hits
$z_0^{\text{track}} \leq 60$ cm
$E/p \leq 2$ unless $p_T \geq 50$ GeV
$\chi^2_{CES} \leq 10$
-3.0 cm $\leq Q \times \Delta X_{CES} \leq 1.5$ cm
$\lvert\Delta Z_{CES}\rvert < 3$ cm
$L_{shr} \leq 0.2$
Conversion Removal

Table 2: Cuts to identify tight central electrons

Programs. These datasets are listed in Appendix A. We remove events that produce a b or c quark from the W/Z + partons samples to avoid overlap with the W/Z + heavy partons samples.

4 Event Selection

Our base sample for the analysis is inclusive W's and Z's. We use the standard CDF cuts [12] to identify hard (> 20 GeV) electrons and muons, with the additional requirement that hard muons have silicon hits. We require tight central electrons and tight muons, described in Tables 2 and 3, as the trigger leg of the W and Z. We consider looser leptons, described in Tables 3 and 4, for the non-trigger leg of Z reconstruction.

We also use these samples to validate the lepton identification because the cross-sections and kinematics are precisely predicted. In particular, the ratio R of W to Z production is predicted to NNLO with a precision of a few percent [13], providing a very precise test of trigger and lepton efficiencies in the Monte Carlo predictions.

4.1 W Selection

The W selection requires a trigger lepton (see Section 3) with $\text{E}_\text{T} > 20$ GeV, $\not\!\!E_T > 25$ GeV, and transverse mass > 20 GeV. The difference in ϕ between the highest-energy lepton and the ϕ of the $\not\!\!E_T$ is required to be greater than 0.5. In addition, electrons are required to satisfy the conversion filter, and muons the decay-in-flight algorithm, as described below.

In addition to passing the kinematic and geometric cuts above, the highest-E_T electron is required to pass a conversion filter. If there is an opposite-sign track that is an electron candidate and has $\Delta \cot\theta < 0.04$ and $|sep| < 0.2$, then the electron is called a conversion.

Muon Cuts
Track must be fiducial to CMU, CMP, or CMX
$E_{EM} \leq 2$ GeV
$E_{HAD} \leq 6$ GeV
$E_{EM} + E_{HAD} \geq 0.1$ GeV for CMIO muons
$\text{Iso}(R = 0.4)/E_T \leq 0.1$
≥ 3 COT axial segments with ≥ 5 hits
≥ 2 COT stereo segments with ≥ 5 hits
≥ 1 Si hit
$z_0^{\text{track}} \leq 60$ cm
if $p_T > 300$ GeV, $n_{transitions} \geq 30$
$d_0 < 0.02$ cm
$\Delta X_{CMU} \leq 3$ cm
$\Delta X_{CMP} \leq 5$ cm
$\Delta X_{CMX} \leq 6$ cm
Loose Muon Cuts
$p_T \geq 10$ GeV
Tight Muon Cuts
Muon must be of type CMUP or CMX
$p_T \geq 20$ GeV

Table 3: Cuts to identify muons.

Loose Central Electron Cuts
$\eta_{\text{Detector}} \leq 1.1$
Track must be fiducial to CES
$E_T \geq 12$ GeV
$E_{HAD}/E_{EM} \leq 0.055 + 0.00045 \times E$
$\text{Iso}(R = 0.4)/E_T \leq 0.1$
$p_T \geq 6$ GeV
≥ 3 COT axial segments with ≥ 5 hits
≥ 2 COT stereo segments with ≥ 5 hits
$z_0^{\text{track}} \leq 60$ cm
$E/p \leq 2$ unless $p_T \geq 50$ GeV
$\chi^2_{CES} \leq 10$
-3.0 cm $\leq Q \times \Delta X_{CES} \leq 1.5$ cm
$\lvert\Delta Z_{CES}\rvert < 3$ cm
$L_{shr} \leq 0.2$

Table 4: Cuts to identify loose central electrons

(See Figure 12 for an illustration of the conversion variables.) However, if its matching conversion leg also has another conversion partner, then the original candidate is called a trident, and therefore passes the conversion filter and is classified as an electron.

In addition to passing the kinematic and geometric cuts described above, a muon must pass the decay-in-flight (DIF) removal algorithm. The DIF algorithm requires the χ^2/d.f. of the track fit to be less than 3 and requires that the impact parameter of the track be less than 0.02 cm. Additionally, for tracks with $p_T > 300$ GeV, it requires $N_{transitions} > 30$. [14]

4.2 Z Selection

The Z selection requires two opposite-sign leptons, of which one is tight (Tables 2 and 3), and the other can be loose (Tables 3 and 4).

4.2.1 $Z \to e^+e^-$

We make plots in two dielectron categories: After selecting a tight electron, we look for either a tight or loose second electron. The predicted and observed numbers of events in both of these categories is summarized separately in Table 5.

Selection	Expected	Observed
W(e, $\not\!\!E_T$)	2571230	2548108
W(μ_{CMUP}, $\not\!\!E_T$)	1289610	1279001
W(μ_{CMX}, $\not\!\!E_T$)	904569	895257
Z(e, e)	156894	160251
Z(e, e_{loose})	25506	28896
Z(μ_{CMUP}, μ_{CMU})	8008	8391
Z(μ_{CMUP}, μ_{CMP})	9736	10433
Z(μ_{CMUP}, μ_{CMUP})	39620	36632
Z(μ_{CMUP}, μ_{CMX})	12893	13547
Z(μ_{CMUP}, μ_{CMIO})	9303	8489
Z(μ_{CMX}, μ_{CMU})	5860	6024
Z(μ_{CMX}, μ_{CMP})	6762	6863
Z(μ_{CMX}, μ_{CMUP})	14162	14467
Z(μ_{CMX}, μ_{CMX})	17245	17906
Z(μ_{CMX}, μ_{CMIO})	5852	5967

Table 5: Event counts in W and Z selection samples, split up by categories of the leading and subleading leptons.

5 QCD Background Estimation Technique

The W boson is identified by the presence of a high energy lepton and missing transverse energy. Events containing jets may emulate this signature; a dijet event, for example, may have large $\not\!\!E_T$ arising from the energy mismeasurement of one jet while the other jet in the event can mimic an electron by leaving a track in the COT associated with an electromagnetic energy deposit. We estimate the contribution from these QCD processes by using a data-derived model for these kind of events [15]. This is accomplished by defining an object that is similar to electrons, but has a much larger rate of contamination from jets, labeled "anti-selected electrons". These objects are then used to create a template which is used to model the QCD background in a fit of the $\not\!\!E_T$ distribution.

5.1 Anti-Selected Electron Definition

Following the technique described in Ref.[15], we modify the standard CDF high-p_T electron identification selections [12] to select objects that are mostly fake electrons. We divide the cuts into two categories, as shown in Table 6. We define the anti-selected electron sample by requiring that prospective objects must pass all kinematic cuts while simultaneously failing at least two of the identification cuts. This sample has similar kinematics to the high-p_T electron sample but has many fewer real electrons present in it.

Kinematic Cuts
$\eta_{\text{Detector}} \leq 1.1$ (central)
Track must be fiducial to CES
$E_T \geq 20$ GeV
$p_T \geq 10$ GeV
$z_0^{\text{track}} \leq 60$ cm
$E/p \leq 2$ unless $p_T \geq 50$ GeV
$\text{Iso}(R = 0.4)/E_T \leq 0.1$
Conversion Removal
Identification Cuts
$E(HAD)/E(EM) \leq 0.055 + 0.00045 \times E$
$\chi^2_{CES} \leq 10$
$L_{shr} \leq 0.2$
$-3.0 \leq Q \times \Delta X_{CES} \leq 1.5$ cm
$\lvert\Delta Z_{CES}\rvert < 3$ cm

Table 6: Central tight electron identification cuts [12] divided into two categories: those that enrich the sample with electrons, referred to as "kinematic", and those that discriminate between electrons and misidentified jets, referred to as "identification".

5.2 Fits to the Missing Transverse Energy Distribution

We obtain the number of events that arise from QCD by fitting the $\not\!\!E_T$ distribution of the data using two templates: an electroweak template obtained from $W+$ jets, $Z+$ jets and diboson Monte Carlo, and a QCD template obtained from the anti-selected electron sample. To obtain the QCD template, we take the anti-selected electron sample and subtract the expected W contamination using the Monte Carlo. Figure 1 shows a fit to the electron data using these two templates for events with $p_T(e) > 20$ GeV, $m_T > 20$ GeV, and $\Delta\phi(\not\!\!E_T, e) > 0.5$. After we obtain the number of QCD events in this sample, we extrapolate this number to the W signal region with $\not\!\!E_T > 25$ GeV. We scale the Monte Carlo electroweak contribution and the data-derived QCD template to the result obtained from the $\not\!\!E_T$ fit in the inclusive W sample.

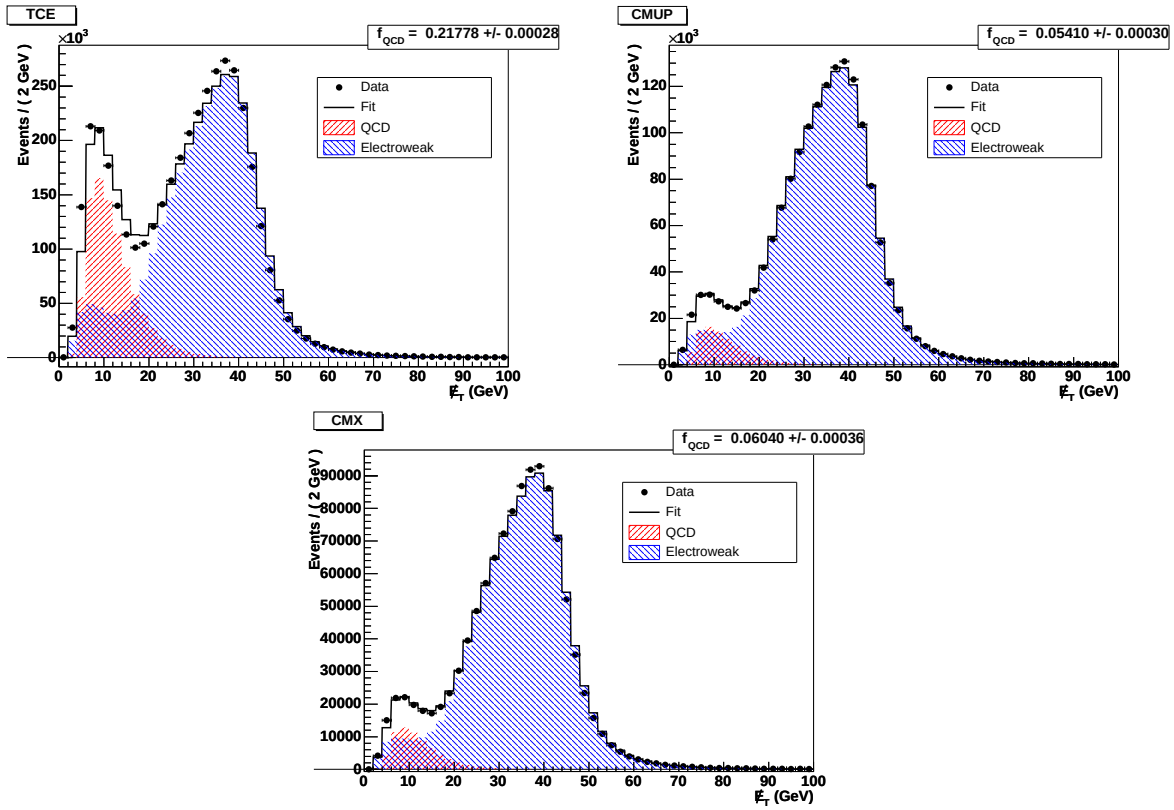

Figure 1: The fits to the $\not\!\!E_T$ distribution of events with $m_T > 20$ GeV and $\Delta\phi(\not\!\!E_T, l) > 0.5$, in each of the three trigger lepton categories. The "Electroweak" template is obtained from Monte Carlo and the "QCD" template is obtained from the anti-selected electron data sample. The fit returns a fraction of the events that are non-electroweak, f_{QCD}.

6 W and Z Sample Validation

6.1 W Sample Validation

We expect 2,571,230 $W \to e\nu$ events versus the observed 2,548,108 events. Table 7 summarizes the predicted numbers of events, and Figure 2 shows the validation plots of kinematic variables in the $W \to e\nu$ sample.

Source	Number of Events
W+light jets	2450327
W+b	7573
W+c	50493
Drell-Yan	23095
$Z \to \tau\tau$	3400
Z+heavy	499
$t\bar{t}$	2113
Diboson	3456
QCD	30277
Expected total	2571230
Observed	2548108

Table 7: Summary of the predictions for $W^{\pm} \to e^{\pm}\nu$. The QCD contribution is estimated as in Sec. 5. The other contributions are calculated from the MC, scaled according to the fit described in Section 5.2.

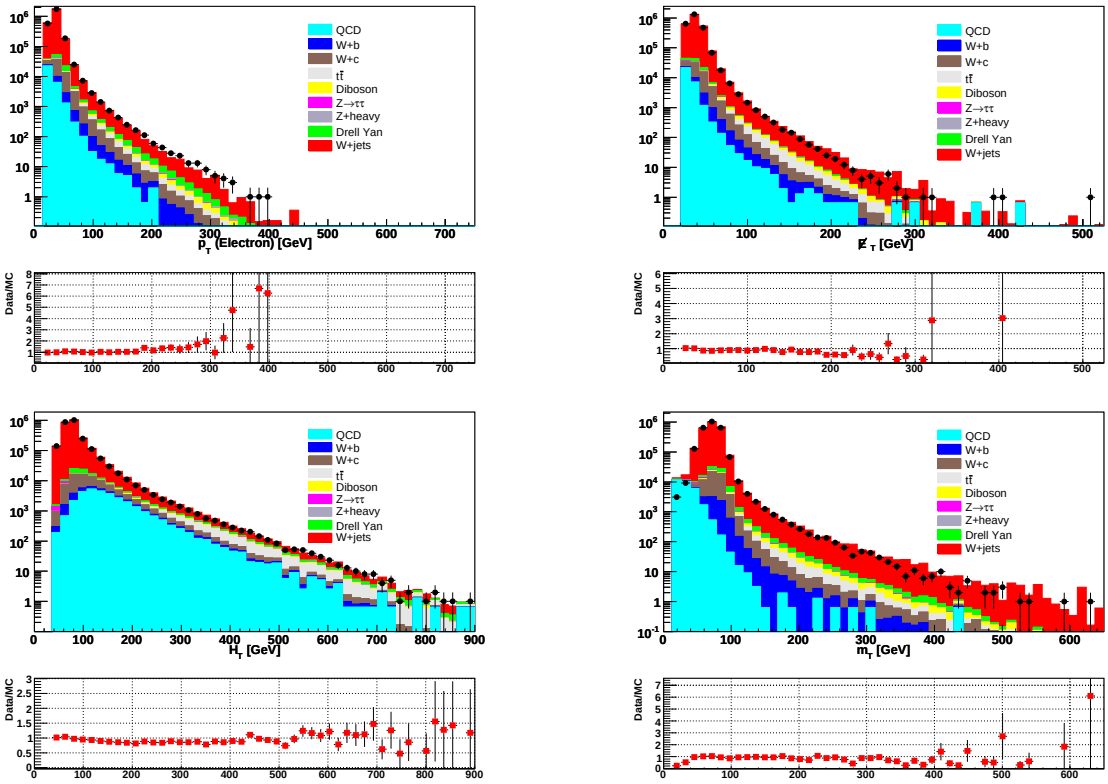

Figure 2: W validation plots, electron trigger: p_T of the highest-p_T good electron, $\not\!\!E_T$ and H_T in the event, M_T of electron and $\not\!\!E_T$. There are cuts requiring $\not\!\!E_T > 25$ GeV and $m_T > 20$ GeV.

6.1.1 $W \to \mu\nu$ events

In CMUP-triggered events, we expect 1,289,610 $W \to e\nu$ events versus the observed 1,279,011 events, while in CMX-triggered events, we expect 904,569 and see 895,257. Tables 8 and 9 summarize the predicted numbers of events, and Figures 3 and 4 show the validation plots of kinematic variables in the $W \to e\nu$ sample.

Source	Number of Events
W+light jets	1139312
W+b	3589
W+c	23691
Drell-Yan	114194
$Z \to \tau\tau$	1708
Z+heavy	1337
$t\bar{t}$	1072
Diboson	1723
QCD	2986
Expected total	1289610
Observed	1279011

Table 8: Summary of the predictions for $W^{\pm} \to \mu^{\pm}\nu$ with a CMUP trigger. The QCD contribution is estimated as in Sec. 5. The other contributions are calculated from the MC, scaled according to the fit described in Section 5.2.

Source	Number of Events
W+light jets	802619
W+b	2337
W+c	15550
Drell-Yan	78109
$Z \to \tau\tau$	1204
Z+heavy	845
$t\bar{t}$	535
Diboson	1023
QCD	2348
Expected total	904569
Observed	895257

Table 9: Summary of the predictions for $W^{\pm} \to \mu^{\pm}\nu$ with a CMX trigger. The QCD contribution is estimated as in Sec. 5. The other contributions are calculated from the MC, scaled according to the fit described in Section 5.2.

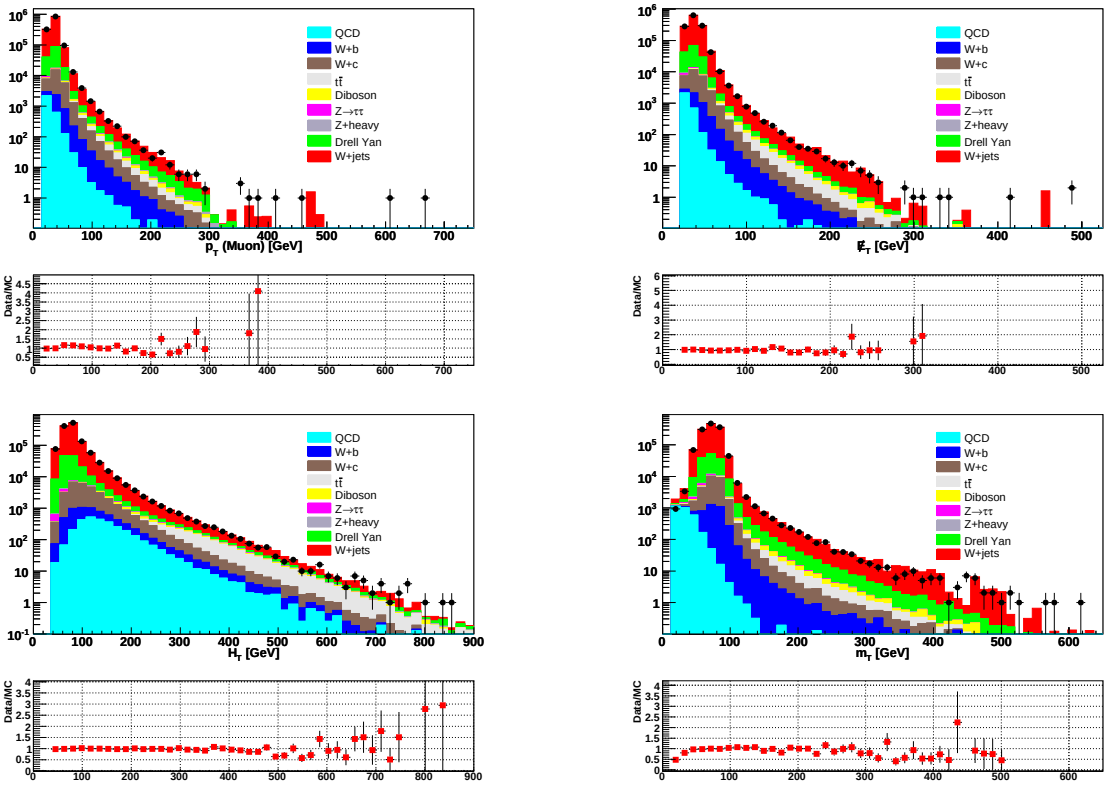

Figure 3: W validation plots, CMUP trigger: p_T of the highest-p_T good muon, $\not\!\!E_T$ and H_T in the event, M_T of the good highest-p_T muon and $\not\!\!E_T$. There are cuts requiring $\not\!\!E_T > 25$ GeV and $m_T > 20$ GeV.

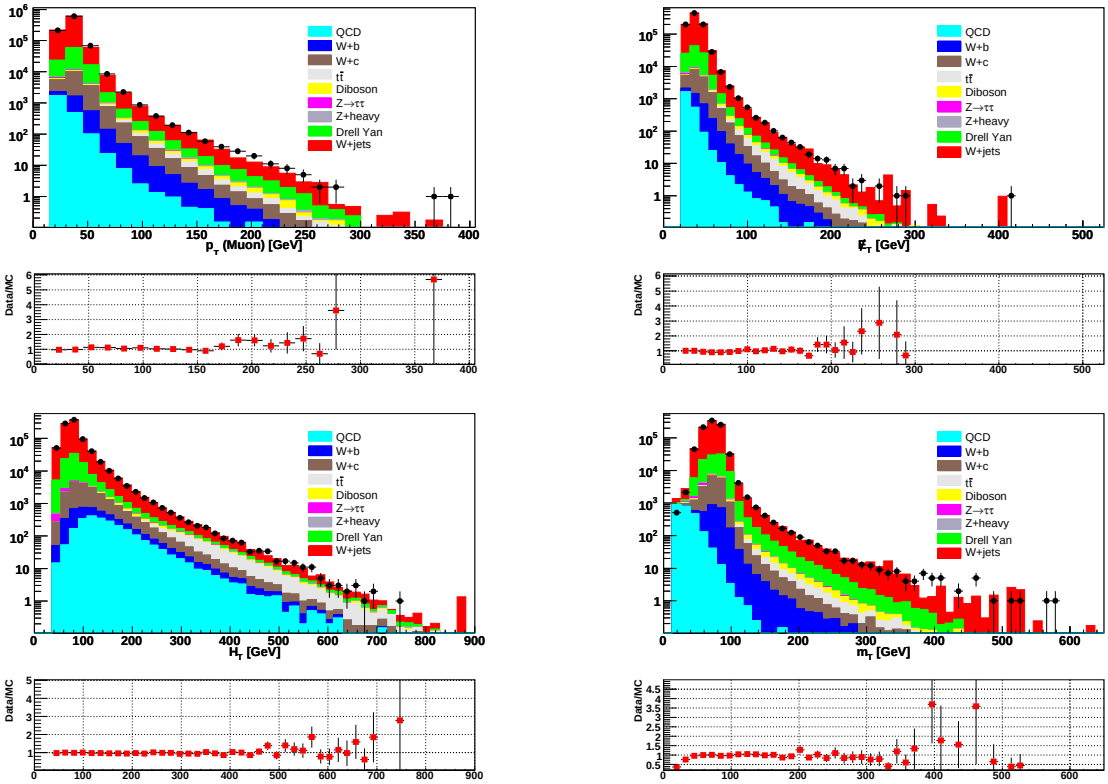

Figure 4: W validation plots, CMX trigger: p_T of the highest-p_T good muon, $\not\!\!E_T$ and H_T in the event, M_T of the good highest-p_T muon and $\not\!\!E_T$. There are cuts requiring $\not\!\!E_T > 25$ GeV and $m_T > 20$ GeV

6.2 Z Sample Validation

Table 10 shows predicted and observed event counts for the full $Z \rightarrow e^+e^-$ sample, and Figure 5 shows validation plots of the same sample.

Source	$N(Events)$ in full range	$N(Events)$ in Z window
W+light jets	63	16
W+b jets	0.9	0.2
W+c jets	5.7	1.8
Drell-Yan	120115	105801
$Z \rightarrow \tau\tau$	752	26
Z+heavy jets	1535	1438
$t\bar{t}$	22	5
Diboson	169	123
QCD	224	154
Expected total	122887	107567
Observed	129462	111063

Table 10: Summary of the predictions and observations for $Z/\gamma^* \rightarrow e^+e^-$ where the trigger is TCE. We show the prediction over the entire range of $m(e^+e^-)$ as well as the prediction in the Z mass window, $76 < m(e^+e^-) < 106$ GeV.

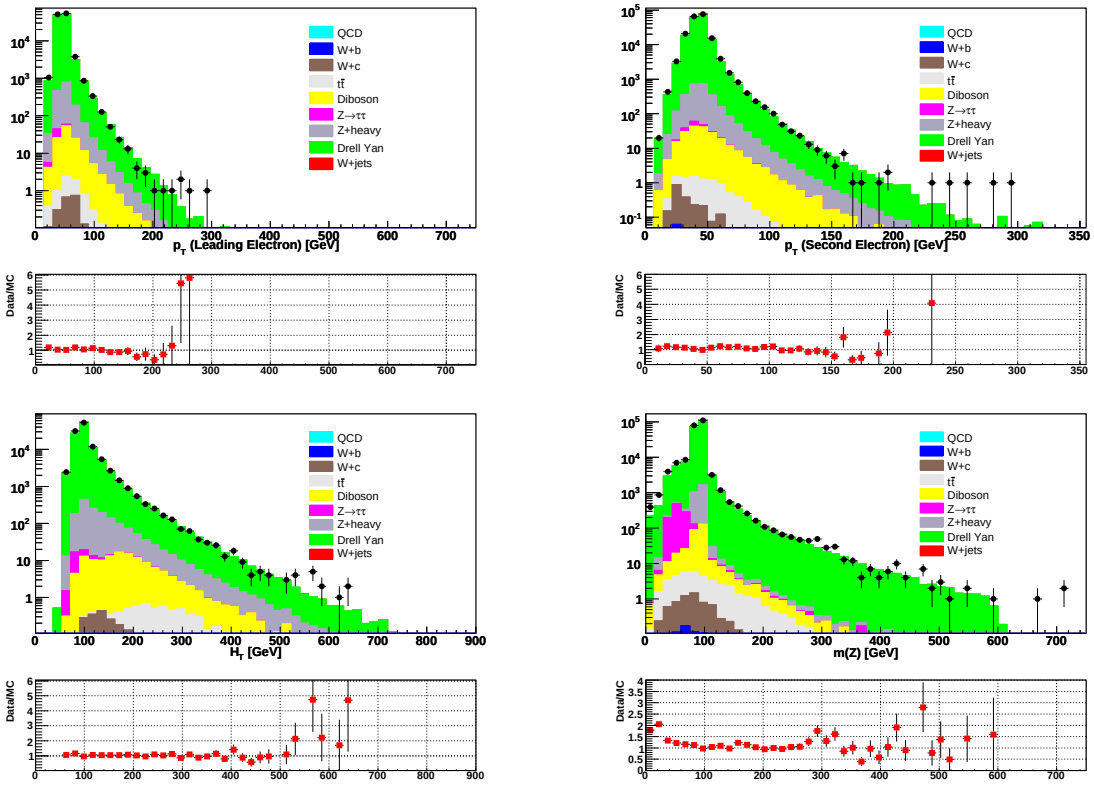

Figure 5: Plots of e-triggered Z events: the p_T of the two leading electrons, the H_T in the event, and the dilepton mass. In all the plots except the mass plot, there is a cut that the dilepton mass is between 76 and 106 GeV.

6.2.1 $Z \to \mu^+\mu^-$

We make predictions in ten dimuon categories. After selecting a tight muon from either a CMUP or a CMX trigger, we look for a second muon in any of the CMU, CMP, CMUP, CMX, or CMIO categories. The predicted and observed numbers of events in each of these categories is summarized separately in Table 5. Tables 11 and 12 show predicted and observed event counts for CMUP-triggered and CMX-triggered $Z \to \mu^+\mu^-$ events, with all five categories of the second muon combined. Figures 6 and 7 show validation plots of the same sample.

Source	$N(Events)$ in full range	$N(Events)$ in Z window
W+light jets	366	73
W+b jets	11	1.8
W+c jets	53	10
Drell-Yan	75970	64783
$Z \to \tau\tau$	653	19
Z+heavy jets	1012	936
$t\bar{t}$	46	8.9
Diboson	131	86
QCD	22	15
Expected total	78263	65933
Observed	75674	60163

Table 11: Summary of the predictions and observations for $Z/\gamma^* \to \mu^+\mu^-$ where the trigger is CMUP muon. We show the prediction over the entire range of $m(\mu^+\mu^-)$ as well as the prediction in the Z mass window, $76 < m(\mu^+\mu^-) < 106$ GeV.

Source	$N(Events)$ in full range	$N(Events)$ in Z window
W+light jets	244	54
W+b jets	6	1.3
W+c jets	34	7.5
Drell-Yan	51634	44448
$Z \to \tau\tau$	417	9.6
Z+heavy jets	658	611
$t\bar{t}$	22	4.4
Diboson	78	52
QCD	17	12
Expected total	53112	45201
Observed	53254	42693

Table 12: Summary of the predictions and observations for $Z/\gamma^* \to \mu^+\mu^-$ where the trigger is CMX muon. We show the prediction over the entire range of $m(\mu^+\mu^-)$ as well as the prediction in the Z mass window, $76 < m(\mu^+\mu^-) < 106$ GeV.

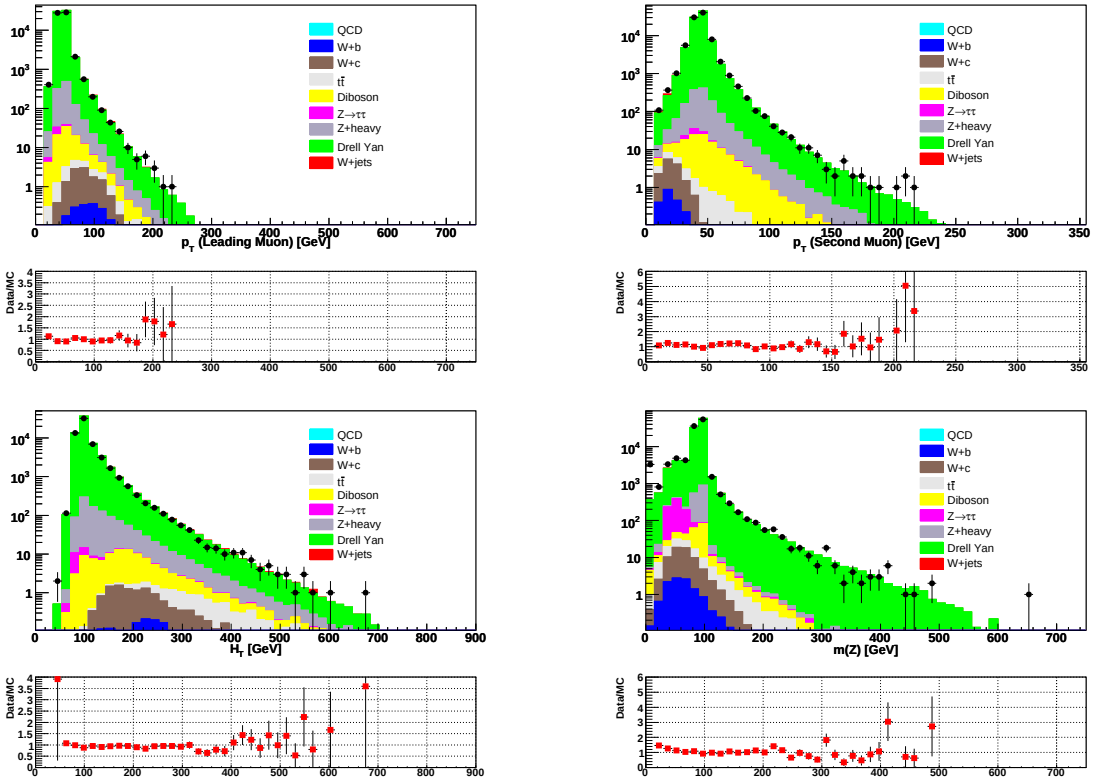

Figure 6: Plots of CMUP μ-triggered Z events: the p_T of the two leading electrons, the H_T in the event, and the dilepton mass. In all the plots except the mass plot, there is a cut that the dilepton mass is between 76 and 106 GeV.

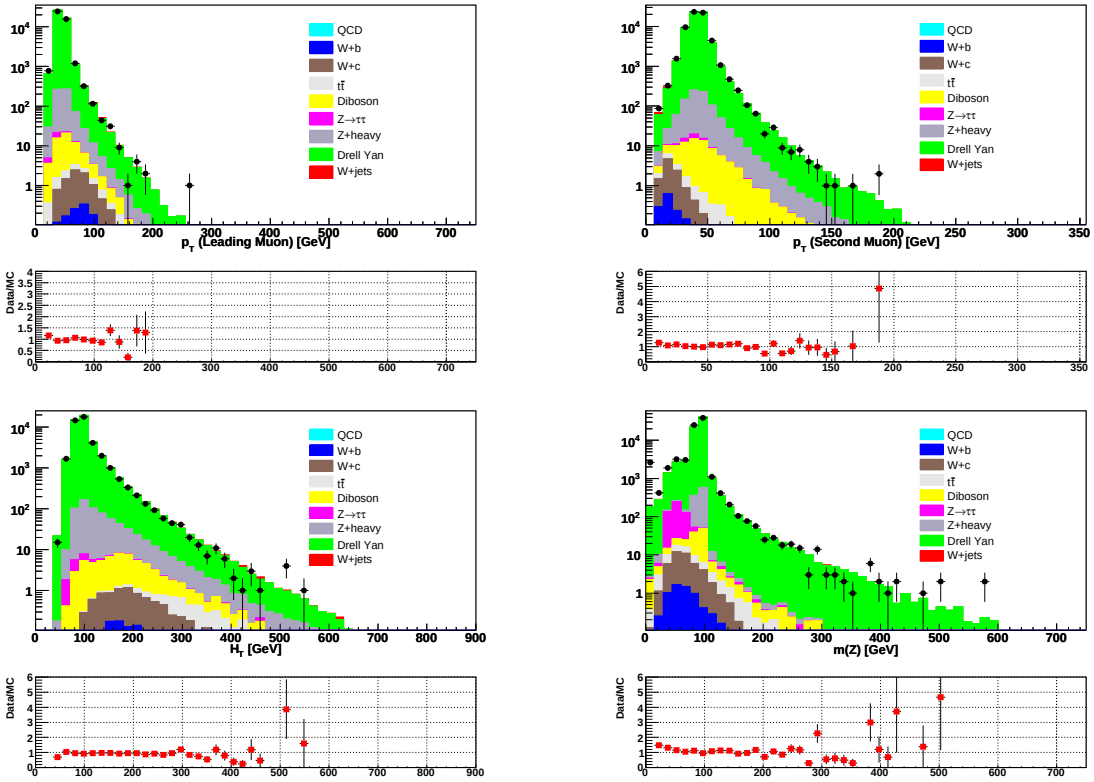

Figure 7: Plots of CMX μ-triggered Z events: the p_T of the two leading electrons, the H_T in the event, and the dilepton mass. In all the plots except the mass plot, there is a cut that the dilepton mass is between 76 and 106 GeV.

Trigger	R	Systematic Uncertainty
TCE	10.84	1.6%
CMUP	11.30	5.9 %
CMX	10.88	2.0%

Table 13: The measured ratio R of W to Z production, and the trigger rate uncertainty we calculate by comparing it to the NNLO calculated value of 10.67.

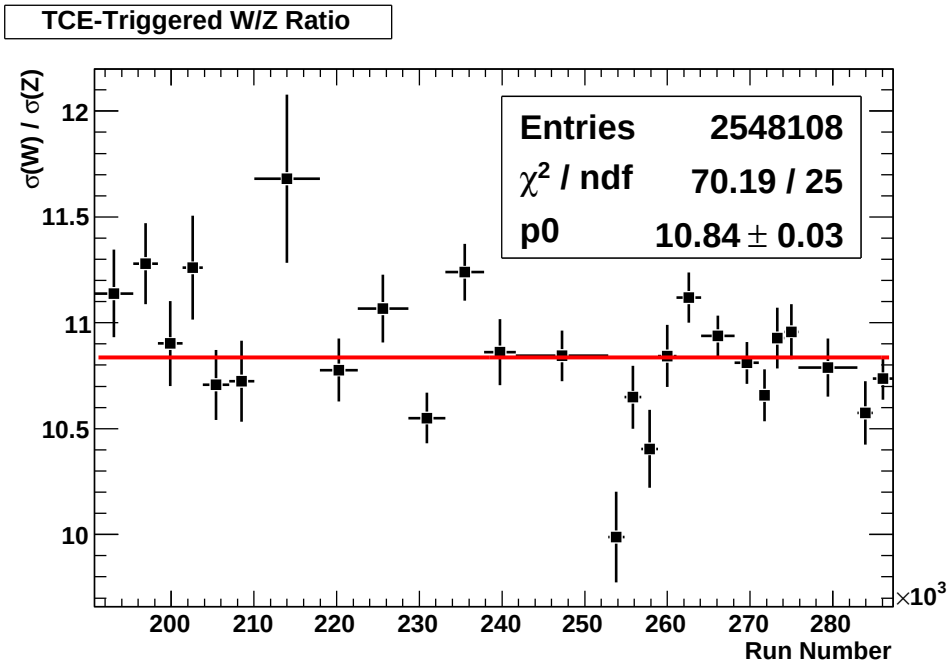

Figure 8: The ratio, R, of W and Z cross sections for each run period, using the electron trigger.

6.3 The Ratio of W to Z Production 'R' as a Precision Check

We use the W and Z cross sections for each run period [16] to validate the datasets. The ratio of W to Z production is a very precise test of problems in lepton trigger efficiencies, lepton identification efficiencies, or problems with $\not\!\!E_T$ [17]. We use the deviation from the theoretical value of $R = 10.67$[13] as a systematic error on the trigger efficiency. Figures 8, 9, and 10 show R versus run number for electron-, CMUP muon-, and CMX muon-triggered events. The fluctuation of R with time is at least partially due to luminosity effects. At higher luminosity, leptons are less likely to pass isolation cuts, decreasing the measured Z cross section more than the W. Table 13 shows the values that we measure and the systematic uncertainties we apply.

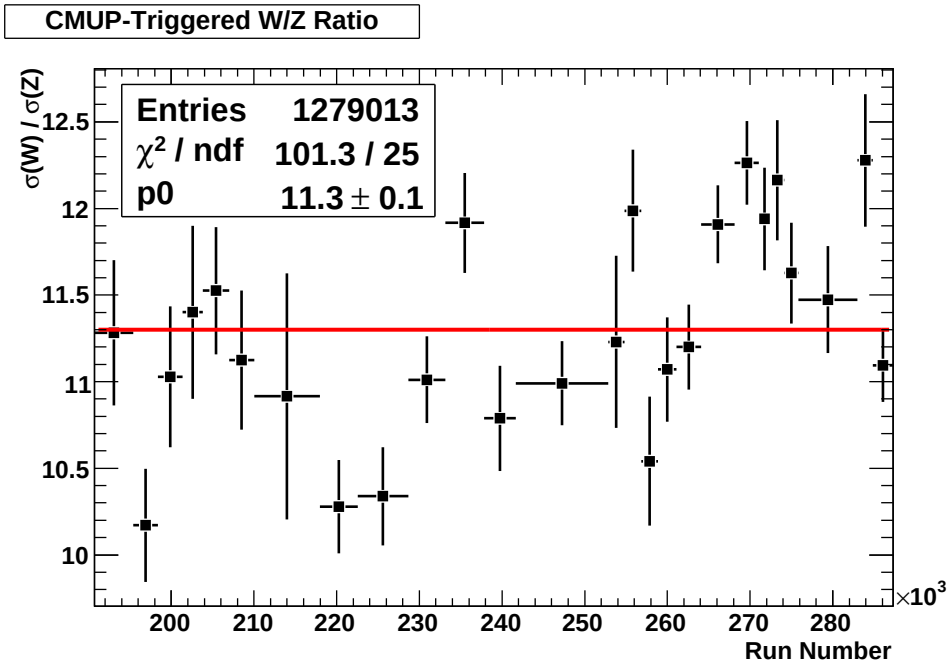

Figure 9: The ratio, R, of W and Z cross sections for each run period, using the CMUP muon trigger.

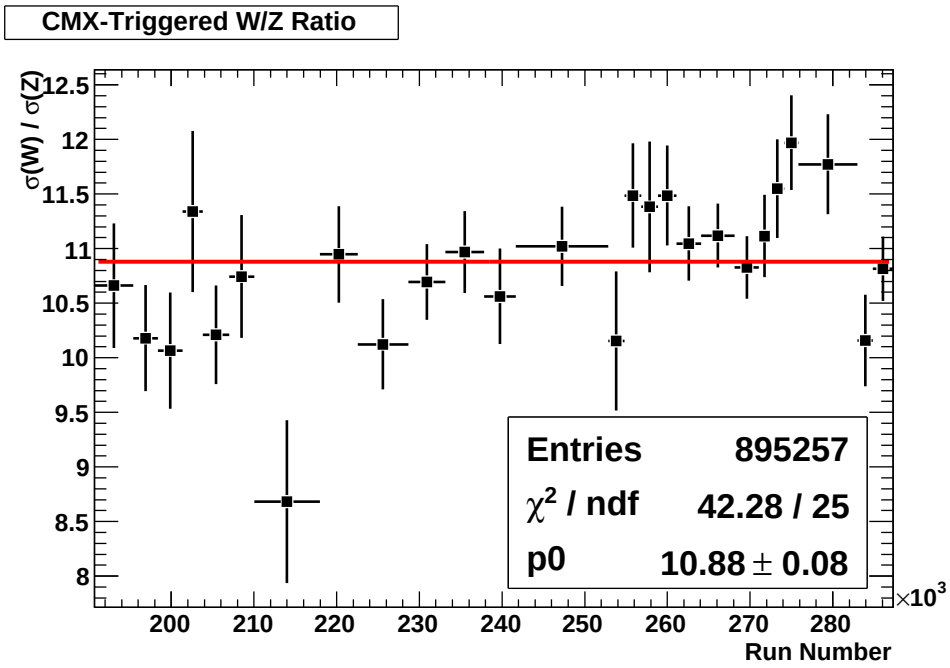

Figure 10: The ratio, R, of W and Z cross sections for each run period, using the CMX muon trigger.

7 Soft Lepton Identification

7.1 Soft Electrons

We identify soft electrons using a method adapted from the B-Group's soft electron tagger [18]. For every track in the event, we require that it passes track quality cuts and fiduciality cuts:

- 20 axial and 20 stereo COT hits
- At least 2 COT superlayers with 6 hits
- Track extrapolates to CES, CPR, and calorimeter
- Track $|\eta| < 1$.

After these cuts, we use a likelihood-based calculator to identify tracks that come from electrons. The likelihood calculator uses seven discriminating variables: $\frac{dE}{dx}$, E_{EM}/P, $\frac{E_{Had}}{E_{EM}}$, E_{CPR}, E_{CES}, ΔX_{CES}, and ΔZ_{CES}, and is trained completely on data without resorting to the Monte Carlo. The CES variables are calculated using the 2-dimensional CES shower algorithm [19]. The calorimeter variables are calculated using a narrow, two-tower wide section of the calorimeter.

We calculate a likelihood for each variable and multiply these likelihoods together to get the final likelihood:

$$\begin{aligned} \mathcal{L}_i &= \frac{\mathcal{L}_i^{real}}{\mathcal{L}_i^{fake}} \\ Q &= \prod_i \mathcal{L}_i \\ \mathcal{L} &= \frac{Q}{1+Q} \end{aligned}$$

We identify a candiate as an electron if it has $\mathcal{L} > 0.99$. The separation in ID rate between real and fake electrons is shown in Figure 11.

7.1.1 Training Sample Selection

We use identified conversions as a training sample of real electrons. Using the 8-GeV electron trigger, we obtain a pure sample of conversions by looking for pairs of tracks that match the following criteria: (see Figure 12 for an illustration of the variables)

- Opposite sign
- $|Sep| < 0.2$ cm
- $\Delta \cot(\theta) < 0.1$

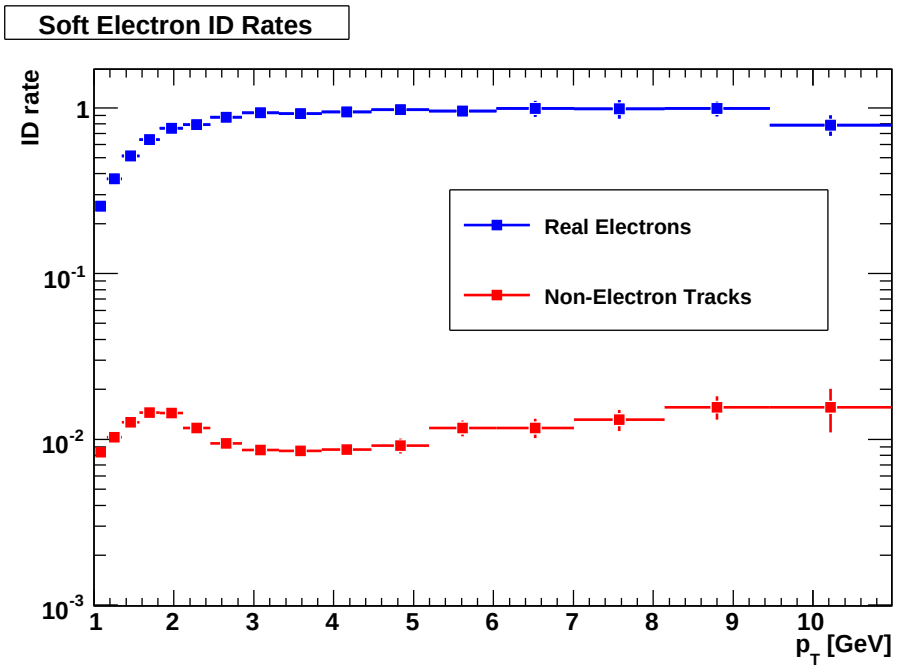

Figure 11: Comparison of the ID rate for real and fake electrons as a function of p_T.

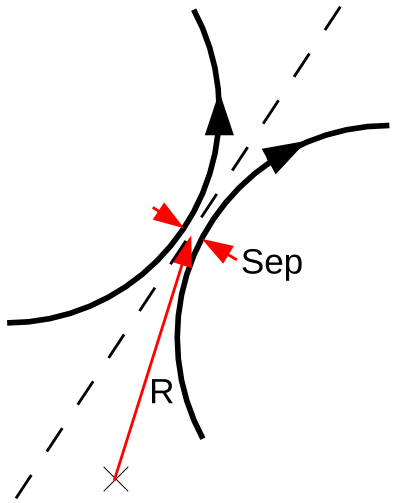

Figure 12: Conversion identification variables

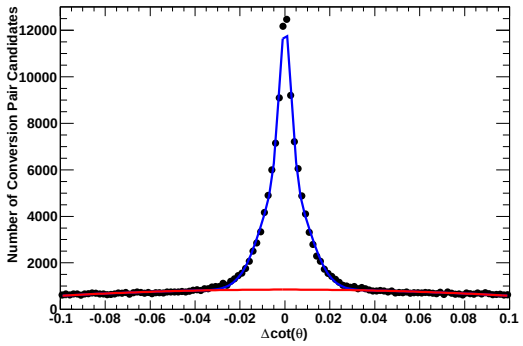

Figure 13: The $\Delta\cot(\theta)$ distribution after the initial conversion identification cuts. The fit is used to estimate the background under the peak, and the sidebands are used to subtract it.

- $R_{Conv} > 8$ cm

After these cuts, we fit the $\Delta\cot(\theta)$ distribution, shown in Figure 13 to determine the non-conversion background under the peak. We use the sideband of the distribution ($0.06 < |\Delta\cot(\theta)| < 0.1$) to subtract out this background.

Since the higher-p_T leg of the conversion will be trigger-biased, we train the likelihood function using the soft leg. We also don't use conversion pairs in which the hard leg extrapolates to the same calorimeter towers that are used for the soft leg, since those conversions have a very different E_{em}/p distribution.

We use generic tracks as the background sample for the likelihood. Using the 20-GeV muon trigger, we eliminate all tracks that pass a conversion filter tuned to reject conversions rather than to find a pure sample:

- Opposite sign
- $|Sep| < 0.2$ cm
- $\Delta\cot(\theta) < 0.03$
- $R_{Conv} > 0$

To further reduce the contamination of this 'fake' sample by real electrons, we ignore all events that have an identified hard electron (using standard CDF cuts) or a SecVtx tag.

7.1.2 Efficiency and Fake Rate Parameterization

The likelihood calculation doesn't work in the Monte Carlo, since it depends on the precise response of the calorimeters at low energy, which isn't modeled very well. Instead, we use the training samples to calculate the efficiency and fake rate of the soft electron identification as a function of p_T, η, and isolation. We apply this efficiency or fake rate to each candidate track in the MC to find the predicted number of identified electrons.

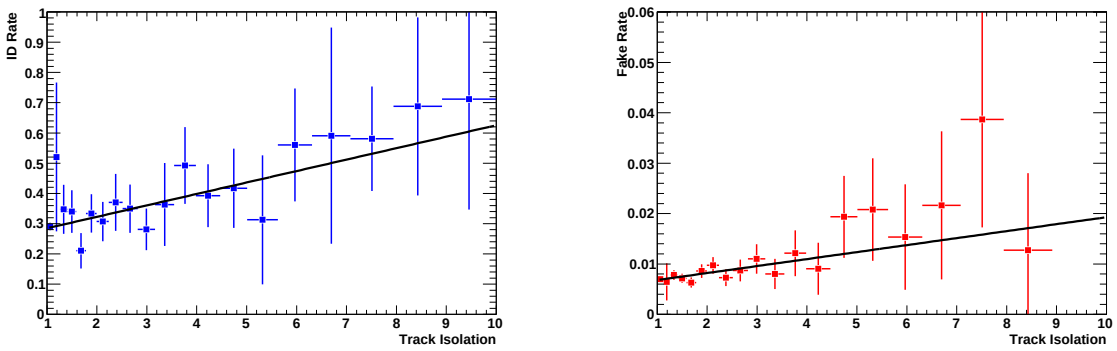

Figure 14: Examples of fits to the soft electron efficiency (left) and fake rate (right) as a function of track isolation in a particular p_T and η bin.

We divide p_T into bins of $1 < p_T < 1.5$, $1.5 < p_T < 2$, $2 < p_T < 2.5$, $2.5 < p_T < 3$, $3 < p_T < 8$, and $8 < p_T < 20$. We divide η into bins of $|\eta| < 0.2$, $0.2 < |\eta| < 0.6$, and $0.6 < |\eta| < 1$. In each of these bins, we fit the efficiency and fake rate to a linear function of the isolation. Some representative fits are shown in Figure 14. To show that this scheme takes into account any correlations between these kinematic variables, the results of applying these parameterizations to the training samples are shown in Figure 15.

7.1.3 Validation

We check the rate parameterization on the `JET50` sample. We take all the generic tracks in the sample, after applying the same electron removal we used for the fake training sample as described in Section 7.1.1. We take the likelihood distribution of all candidate tracks and fit it to the real and fake likelihood templates obtained from the training samples to get the fraction of real and fake electrons in the sample. We find that the sample is 2.5% real electrons. We then check that the predicted ID rate agrees with the actual ID rate.

We use the disagreement between the expected and observed ID rates as a systematic error. We calculate an expected 6448 identified electrons in this sample, and we observe 6345, a difference of 1.6%. However, we assign a systematic uncertainty of 15% to the electron ID rates in order to cover the shape disagreement in p_T and η, as seen in Figure 16. We apply this systematic separately to the real identification and misidentification rates.

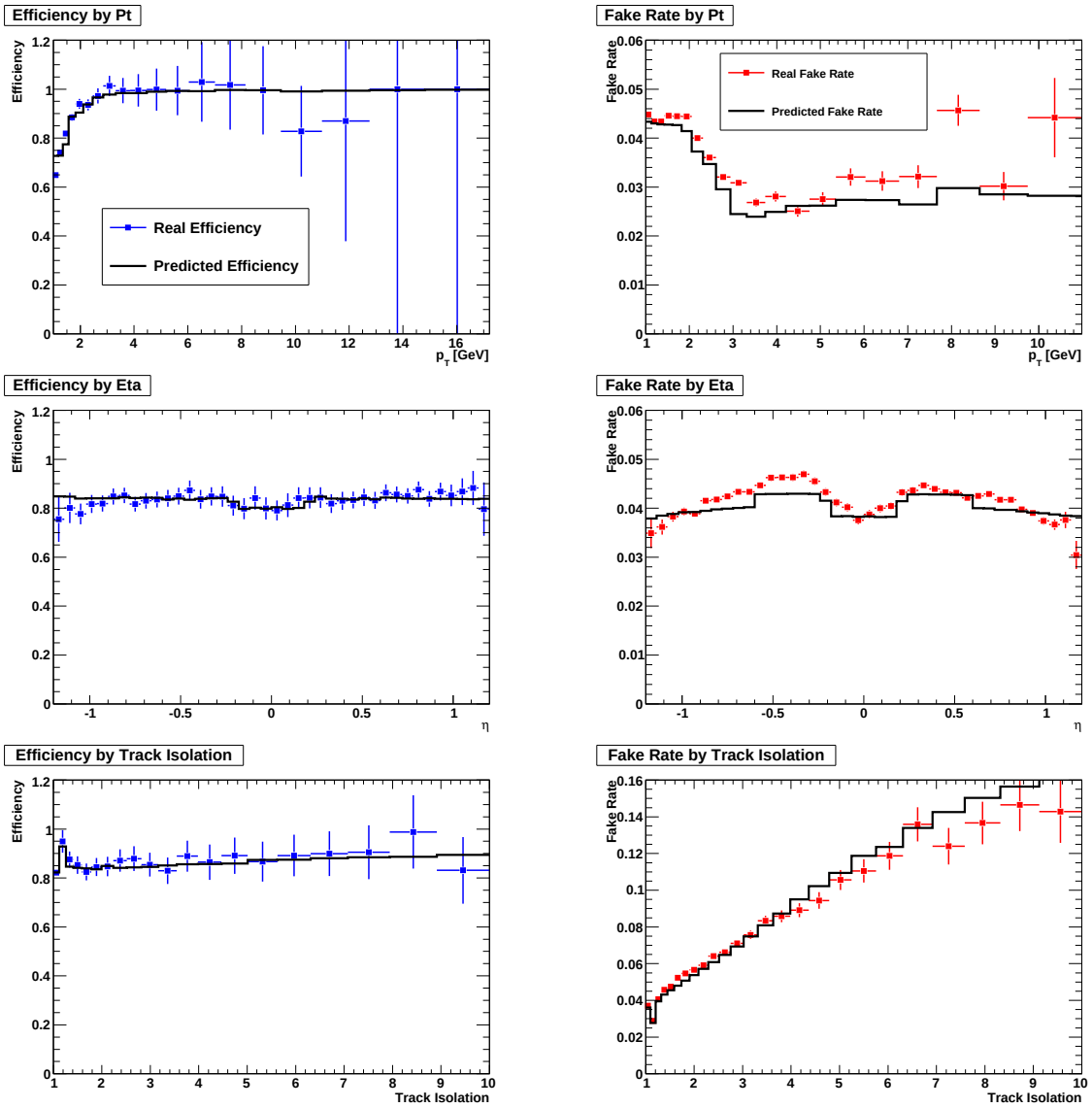

Figure 15: The effect of applying the efficiency and fake rate prediction to the training samples.

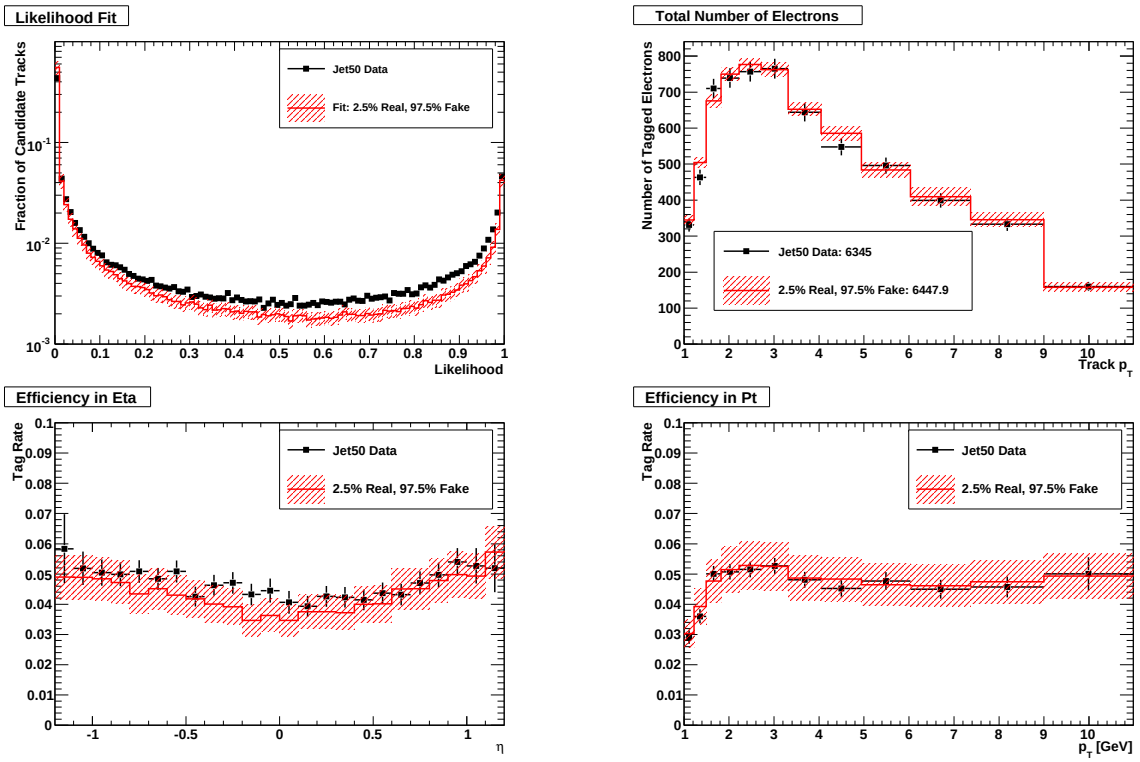

Figure 16: Validation plots of the soft electron fake matrix. Shown is the fit to the likelihood distribution in the jet sample, and the result of applying this mixture of "real" and "fake" to the p_T and η ID rates. We assign a 15% systematic error to the ID rates; this is shown in the plots.

7.2 Soft Muons

We have ported the soft muon identification algorithm described in Ref. [20] from the TopNtuple framework to the Stntuple framework with minimal modifications. We measure the efficiency of the ported identification software using reconstructed $J/\psi \to \mu^+\mu^-$ decays to obtain pure μ samples. The misidentification rates of π and K are measured in $D^{*+} \to D^0\pi^+$ decays where D^0 decays as $D^0 \to K^-\pi^+$. Similarly, the p misidentification rate is measured in $\Lambda^0 \to p\pi$. First, we briefly summarize the algorithm.

7.2.1 Identification Algorithm and Candidate Selections

The soft muon identification algorithm relies on the measured values of track-to-stub matching variables. The list of all such variables is:

- CMU dx,
- CMU dz,
- CMU $d\phi$,
- CMP dx,
- CMP $d\phi$,
- CMX dx,
- CMX dz,
- CMX $d\phi$.

Each of these variables can only be used if a stub exists in the corresponding system, i.e. CMP dx and $d\phi$ only have values if there is a CMP stub.

We make a simple sum Q of χ^2 terms built from these track-to-stub matching variables,

$$Q = \sum_i^n \frac{(x_i - \mu_i)^2}{\sigma_i^2} = \sum_i^n y_i^2, \tag{1}$$

where μ_i and σ_i^2 are the expected mean and variance of the distribution of x_i. If the y_i are independent and normally distributed, the distribution of Q is χ^2 with a mean of n and $\sigma^2 = 2n$. We make the final likelihood by normalizing Q,

$$\mathcal{L} = \frac{Q - n}{\sigma(Q)}, \tag{2}$$

where $\sigma^2(Q)$ is the variance of Q. Additionally, if a track extrapolates to a chamber and a stub is not found, we apply a penalty of $+10$ to $\mathcal{L}$, as in Ref. [20].

The track-to-stub matching variance functions, σ_i in Eq. 1, are copied from the TopNtuple code directly into the Stntuple port with no modifications. The $\sigma(Q)$ term in the denominator of Eq. 2 is decomposed as in Ref. [20]

$$\sigma^2(Q) = 2n + \sum_{i,j} \rho(y_i^2, y_j^2), \tag{3}$$

Soft Muon Candidate Selections
$N(\text{COT}) \geq 48$
$N(\text{COT Axial}) \geq 24$
$N(\text{COT Stereo}) \geq 24$
$\lvert d_0 \rvert < 0.3$ cm, where d_0 is the impact parameter with respect to the beamline
$\lvert z_0 \rvert < 60$ cm
The track must extrapolate to within the physical boundary of a muon chamber.
Identified Soft Muon Requirement
$\lvert \mathcal{L} \rvert < 3.5$

Table 14: Soft muon candidate selections and final likelihood cut used to declare candidate as "identified".

and the ρ's are taken from the TopNtuple code.

Table 14 lists the requirements placed on soft muon candidate tracks as well as the final cut on the likelihood applied to identified soft muons. The cuts on the number of COT hits reduce the background from poorly measured tracks, while the cut on impact parameter removes some of the pion and kaon decay-in-flight background. Note that the fiducial definition described in the last bullet point differs from the one used in Ref. [20]. In that algorithm, candidates were declared fiducial if they extrapolated to within $3\sigma_{MS}$ outside of the physical chamber boundary, where σ_{MS} is the width of the multiple scattering distribution for a given p_T. This change was made due to the unavailability of the extrapolated track-to-chamber boundary distance in the Stntuple format.

The final selection for all identified soft muons is that $|\mathcal{L}| < 3.5$. Note that this means that any candidate that is missing an expected stub is rejected because the likelihood penalty of +10 will cause $|\mathcal{L}| > 3.5$. Therefore, all identified soft muons *must* have stubs in the detector(s) to which the track extrapolates. For example, if a track should cross the physical volume of both the CMU and CMP detectors, there must be stubs in both detectors for it to be identified as a soft muon.

7.2.2 Efficiency and Misidentification Rate Measurements

We use samples of $J/\psi \to \mu^+\mu^-$ to measure the efficiency of the soft muon identification. These samples are obtained from the `jbmu0d`, `jbmu0h`, and `jbmu0i` datasets. We reconstruct the J/ψ by requiring that the trigger muon make a vertex with another track of opposite charge that has an associated object in the muon block. All track requirements listed in Sec. 7.2.1 are applied to both tracks. We further require that the candidate mass be $2.9 < m(\mu\mu) < 3.3$ and that $|\Delta z| < 5$ cm where Δz is the z difference between the two tracks. We define signal and sideband regions as follows:

- Left Sideband: $2.94 < m(\mu\mu) < 3.0$ GeV,
- Signal Region: $3.03 < m(\mu\mu) < 3.15$ GeV,
- Right Sideband: $3.18 < m(\mu\mu) < 3.24$ GeV,

and fit for the signal and sideband yields in bins of p_T of the non-triggered leg. These fits are shown in Fig. 17.

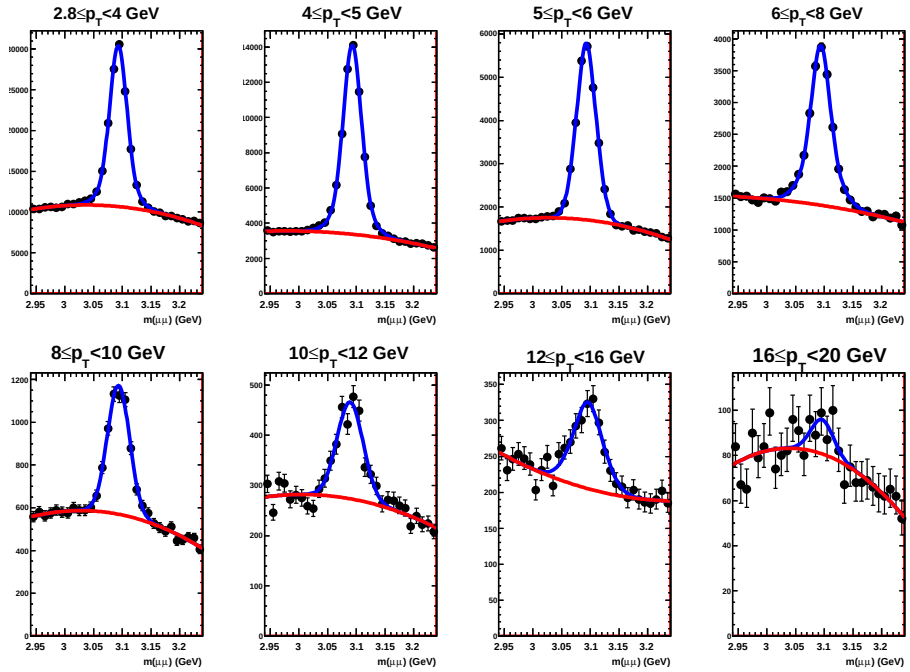

Figure 17: Results of the J/ψ mass fits in bins of the p_T of the softer, not-triggered, candidate leg of the J/ψ.

We obtain pure π and K samples from D^* decays, as mentioned in Sec. 7.2. D^*'s are obtained from the two-track-trigger sample and are reconstructed with the following selections:

- the K must have opposite charge to each of the two π's,
- $|z| \leq 5$ cm between any two tracks,
- the soft pion from the $D^* \to D^0$ decays must have $p_T \geq 500$ MeV,
- the kaon and pion from the D^0 decay must have $p_T \geq 2$ GeV,
- the kaon and pion from the D^0 decay must have $|d_0| \leq 0.2$ cm,
- $m(K\pi) - m(D^0) \leq 30$ MeV where $m(D^0)$ is the nominal D^0 mass,
- $p_T(D^0) \geq 5$ GeV,
- the impact parameter significance of the D^0 is required to be $d_0/\sigma(d_0) \geq 2$,
- $p_T(D^*) \geq 6$ GeV,
- $\Delta m = m(D^*) - m(D^0) \leq 170$ MeV.

- $\chi^2 \leq 100$ where χ^2 is from the vertex fit.

The π and K from the D^0 are required to form a vertex while the slow π from the D^* is attached to the primary vertex. The D^0 vertex is required to point back to the primary vertex. We define sideband and signal regions as follows:

- Left Sideband: $0.1396 < \Delta m < 0.141$ GeV,
- Signal Region: $0.14242 < \Delta m < 0.148421$ GeV,
- Right Sideband: $0.152 < \Delta m < 0.1625$ GeV,

and fit for the signal and sideband yields in bins of p_T of the π or K from the D^0. These fits are shown in Fig. 18.

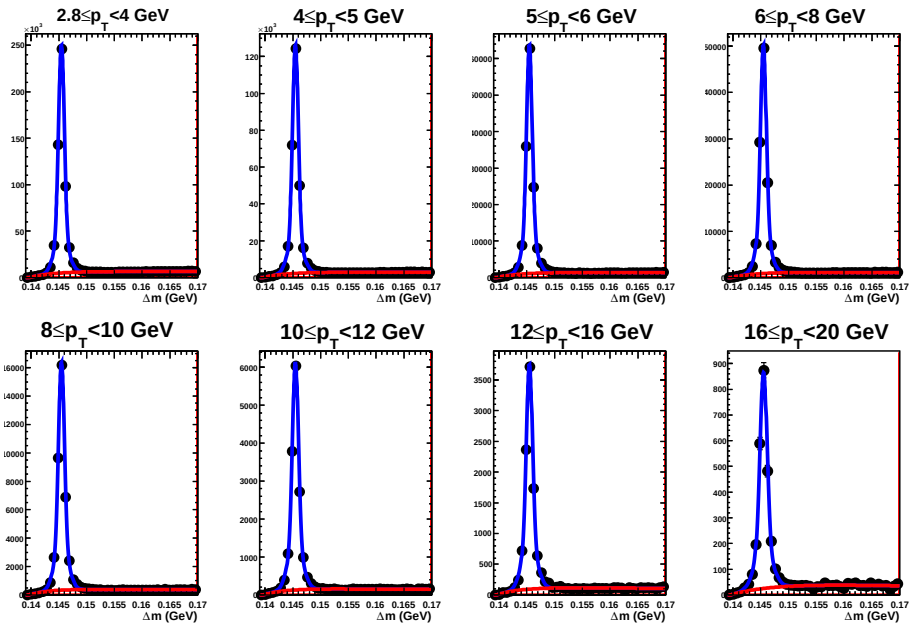

Figure 18: Results of the D^* mass fits in bins of the p_T of candidate π's coming from $D^0 \to K\pi$.

Samples of protons are obtained from $\Lambda \to p\pi$ decays taken from the two-track-trigger dataset. The selections are as follows:

- the two tracks must pass the selections in Sec. 7.2.1,
- the two tracks are required to have opposite charge and fit to a vertex,
- $|\Delta z| \leq 2$ cm between the two tracks,
- the χ^2 of the vertex fit is required to be < 10,
- the decay length significance of the vertex is required to be $L_{xy}/\sigma(L_{xy}) \leq 20$,

- the Λ impact parameter is required to be $|d_0| < 0.02$ cm,
- $1.0 < m(\Lambda) < 1.16$ GeV.

We define sideband and signal regions as follows:

- Left Sideband: $1.101 < m(\Lambda) < 1.106$ GeV,
- Signal Region: $1.111 < m(\Lambda) < 1.121$ GeV,
- Right Sideband: $1.126 < m(\Lambda) < 1.131$ GeV,

and fit for the signal and sideband yields in bins of proton p_T. These fits are shown in Fig. 19.

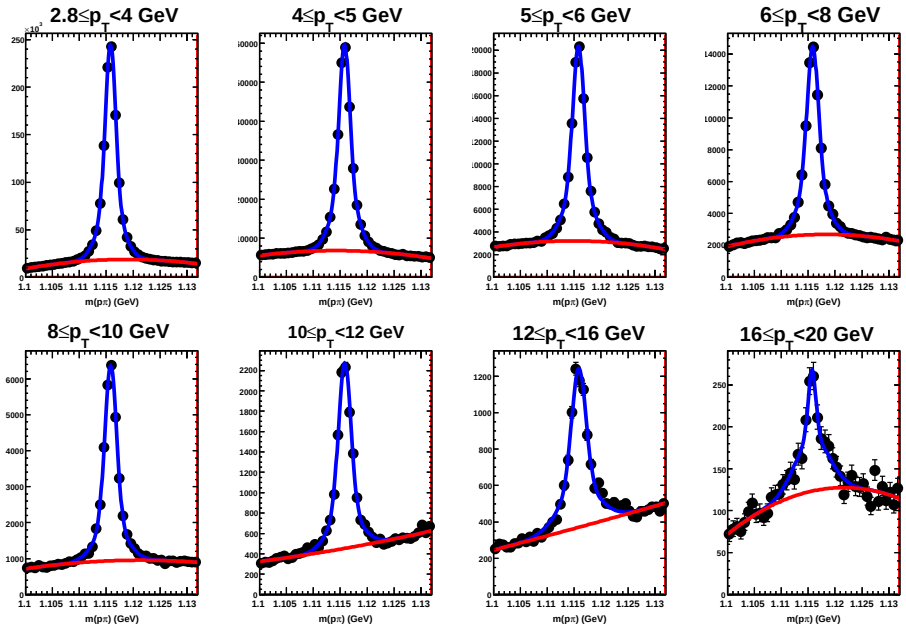

Figure 19: Results of the Λ mass fits in bins of the p_T of candidate p's.

Figure 20 shows the likelihood distributions for μ, π, K, and p obtained from the signal regions in the samples described above. We see that the μ likelihood peaks more strongly at small $\mathcal{L}$ as expected. The final selection, as described in Sec. 7.2.1, is $|\mathcal{L}| < 3.5$.

We follow the technique described in Ref. [21] to obtain the efficiency and fake rates. The identification rate is determined as,

$$R_S = \frac{R_M - R_B \cdot f_B}{1 - f_B}, \tag{4}$$

where R_M and R_B are the identification rates measured in the signal and sideband regions, respectively, and f_B is the background fraction in the signal window. For fake rates, we can write the measured misidentification rate, R_M, in terms of the decay-in-flight rate as,

$$R_M = f_M \cdot R_{DIF} + (1 - f_M) \cdot R_{PT}, \tag{5}$$

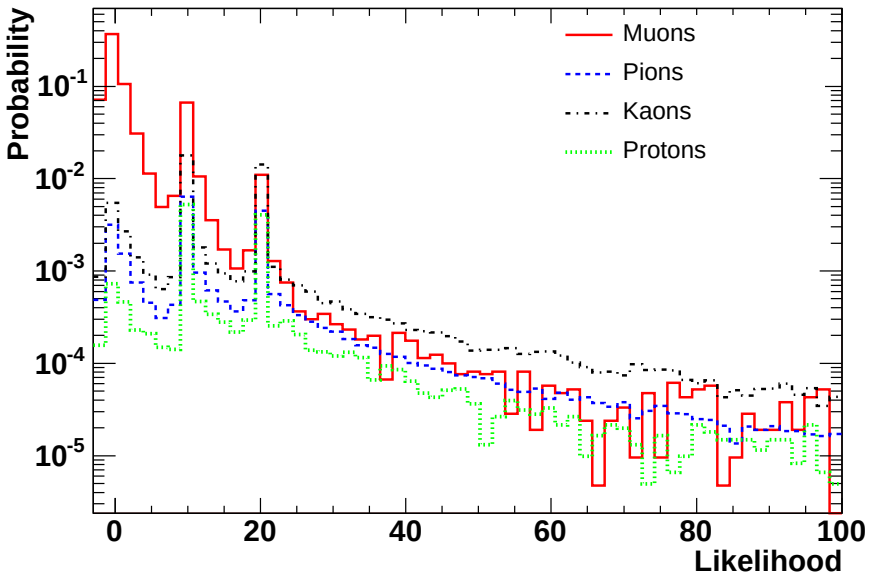

Figure 20: A comparison of the soft muon likelihood distributions for μ, π, K, and p.

where f_M is the decay-in-flight fraction and R_{DIF} and R_{PT} are the identification rates for decay-in-flight and punch-through, respectively. We use the R_{DIF} as presented in Ref. [21].

The identification efficiency is defined as $N(\text{identified})/N(\text{candidates})$, where the candidate requirements are shown in Table 14. The efficiencies for each particle type are plotted in Fig. 21 as a function of p_T. Note that for all particles except for muons, the "efficiency" is actually the rate that the particle is *misidentified* as a muon. We see strong separation between μ and backgrounds.

We make an efficiency matrix in bins of p_T and η using the J/ψ sample. Because the sample is limited in statistics for $p_T > 12$ GeV, we fill in empty bins using fits to the efficiency as a function of p_T for three different η ranges. These fits apply the soft muon identification to Z events so that the region between the J/ψ and Z p_T may be correctly fitted. Figure 22 shows the fit for candidates with $|\eta| < 0.15$. Figure 23 shows the fit for candidates with $0.15 < |\eta| < 0.55$. Figure 24 shows the fit for candidates with $|\eta| > 0.55$. The final μ efficiency matrix is shown in Fig. 25.

For the corresponding binned misidentification matrix, we combine the π, K, and p matrices in the proportion found in W decays as presented in Table 3 of Ref. [21]. These weights are $f(\pi) = 0.719$, $f(K) = 0.156$, and $f(p) = 0.125$. The binned misidentification matrix is shown in Fig. 26.

7.2.3 Soft Muon Systematic Uncertainty Determination

We estimate separate systematic uncertainties for the true μ identification efficiency and the misidentification rate. The sideband subtraction technique used to obtain the μ efficiency matrix introduces uncertainties arising from the statistics of the J/ψ sample. These

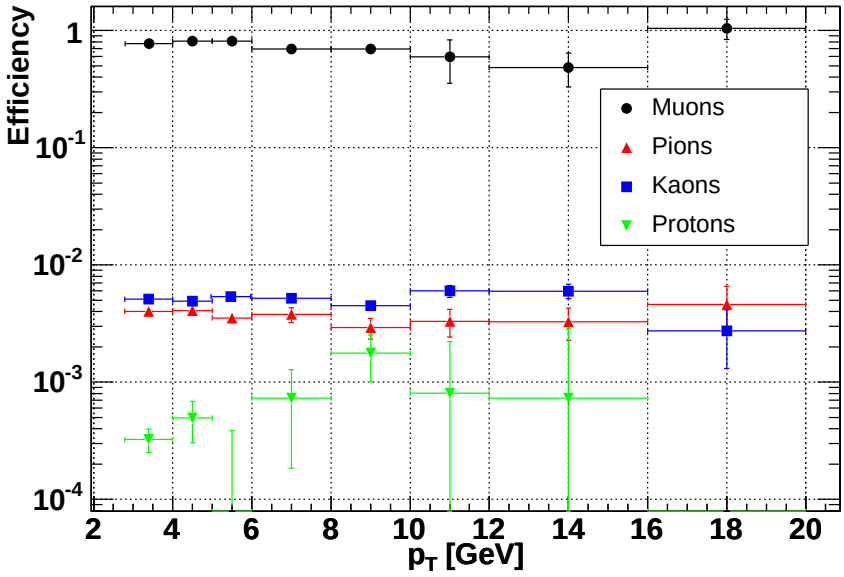

Figure 21: Identification efficiency as a function of p_T for μ, π, K, and p. For the case of the μ, this is the rate at which real muons are identified. For the other species, it is the rate that the particle is misidentified as a muon.

uncertainties vary with p_T and η and are presented as a fraction of the central value in Fig. 27. In addition, we take the maximum variation of 8% arising from the isolation-dependent efficiency shown in Fig. 28 as an uncertainty representing the maximum possible difference between the J/ψ sample environment and the W/Z environment. This is added in quadrature to the statistical uncertainty arising from the sideband subtraction method to obtain the final μ efficiency uncertainty.

The misidentification systematic uncertainty is obtained by selecting μ-free regions in JET samples and taking the difference between observed and predicted soft μ misidentification rates. The JET sample selections are as follows:

- At least 3 jets with L5 corrected $E_T > 15$ GeV and $|\eta| < 2.0$,
- Reject jets with positive SECVTX tag or negative SECVTX tag having $m(SV) > 0.3$ GeV,
- Reject candidate tracks in jets having $d_0/\sigma(d_0) > 2$.

Figure 29 shows the predicted and observed identification rate in JET50 and Fig. 30 shows the same in JET100.

The differences between the predicted and observed number of events are shown in Table 15. We take twice the largest error as the systematic uncertainty on the misidentification rate.

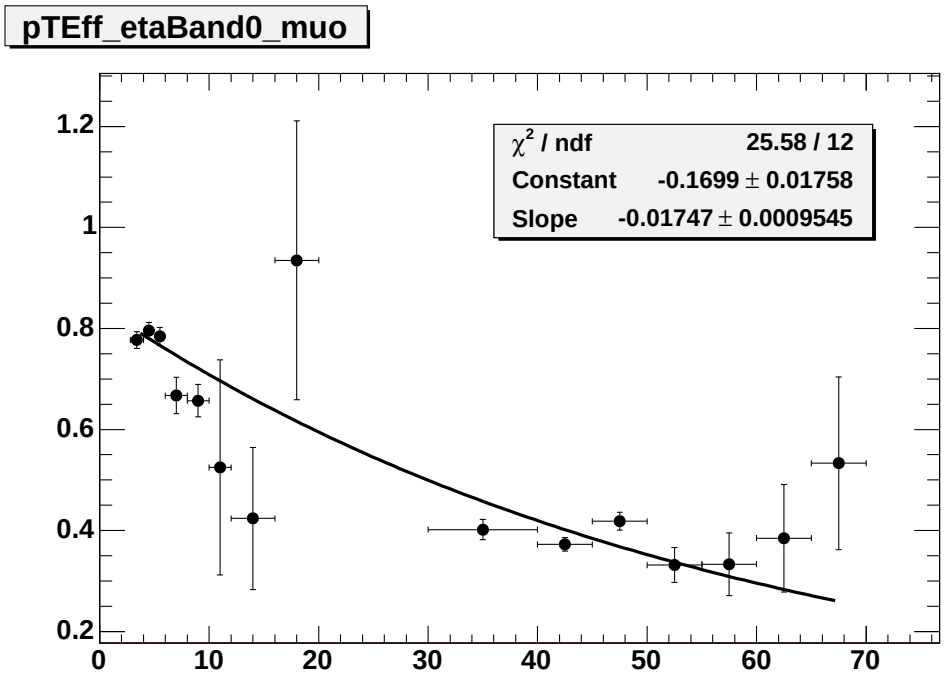

Figure 22: Fit for soft muon efficiency function over J/ψ and Z events in the η range $|\eta| < 0.15$.

Sample	Identified	Predicted	Uncertainty
JET50	517	505	2.3%
JET100	2331	2220	4.8%

Table 15: Number of events predicted by applying the soft muon misidentification matrix and observed in JET50 and JET100 data.

7.2.4 Application of Soft Muon Identification to W/Z Samples

We apply additional selection to soft muon candidates when we run the algorithm on our high p_T W/Z data samples. Any track already identified as a μ in the W or Z selection is ignored. We require $N(\text{SVX}) > 0$, $3 < p_T < 20$ GeV, $|\eta| < 1.2$, and that the track be inside of a reconstructed jet having $|\eta| < 2.0$ and Level 5 corrected energy of $E_T > 5$ GeV. Any track that is identified as a conversion partner is rejected. We require that the track candidate have $|\Delta z| < 5$ cm with respect to the high p_T trigger lepton. If the trigger lepton is a μ, we form the invariant mass of the candidate + trigger, M, under the hypothesis that the candidate is a muon and then reject the following:

- $M < 5$ GeV to remove the $b\bar{b}$ background.
- Candidates in a jet having $f_{EM} > 0.8$ with the candidate track being the only track in the jet with $p_T > 1$ GeV, where f_{EM} is the electromagnetic fraction. This cut rejects radiative μ events.
- $9 < M < 10$ GeV if the candidate track has opposite charge to the trigger muon. This

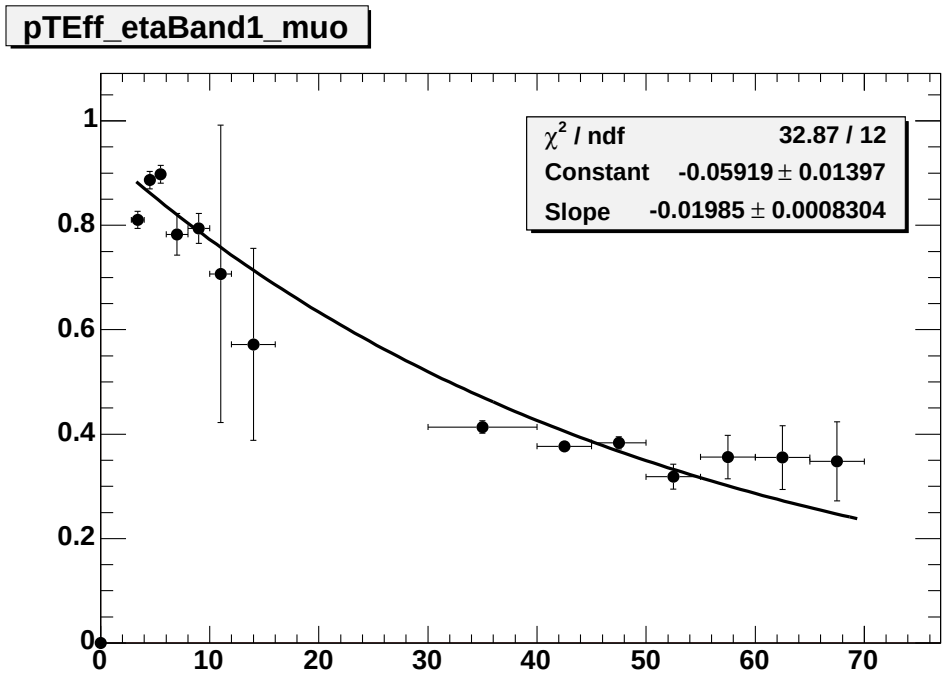

Figure 23: Fit for soft muon efficiency function over J/ψ and Z events in the η range $0.15 < |\eta| < 0.55$.

rejects Υ events.

- $80 < M < 100$ GeV if the candidate track has opposite charge to the trigger muon. This rejects Z events.

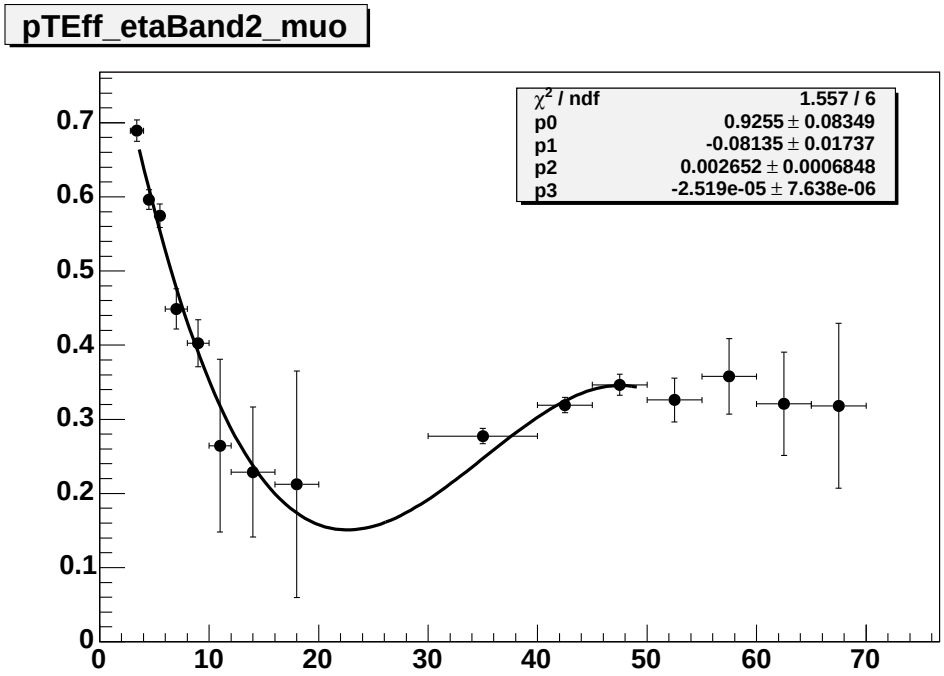

Figure 24: Fit for soft muon efficiency function over J/ψ and Z events in the η range $|\eta| > 0.55$.

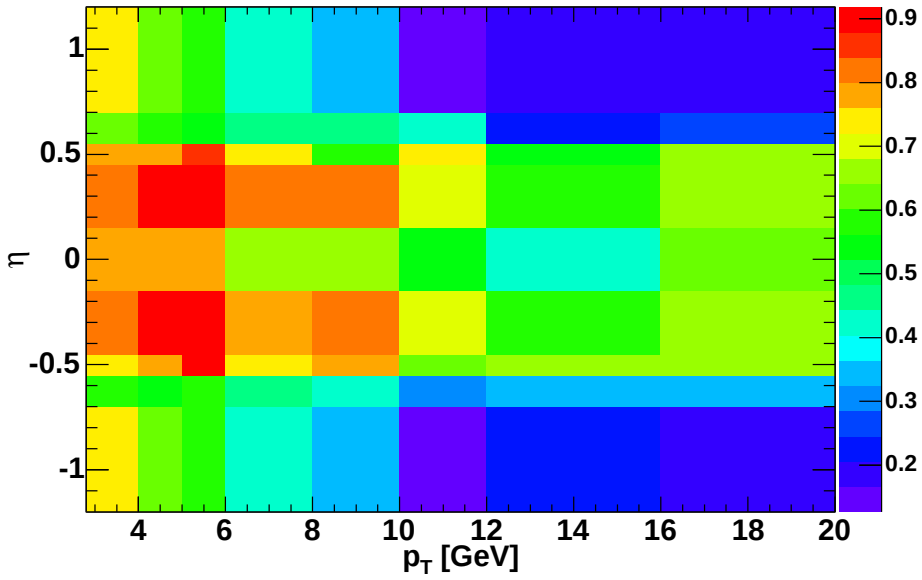

Figure 25: Soft muon ID rate matrix in bins of p_T and η.

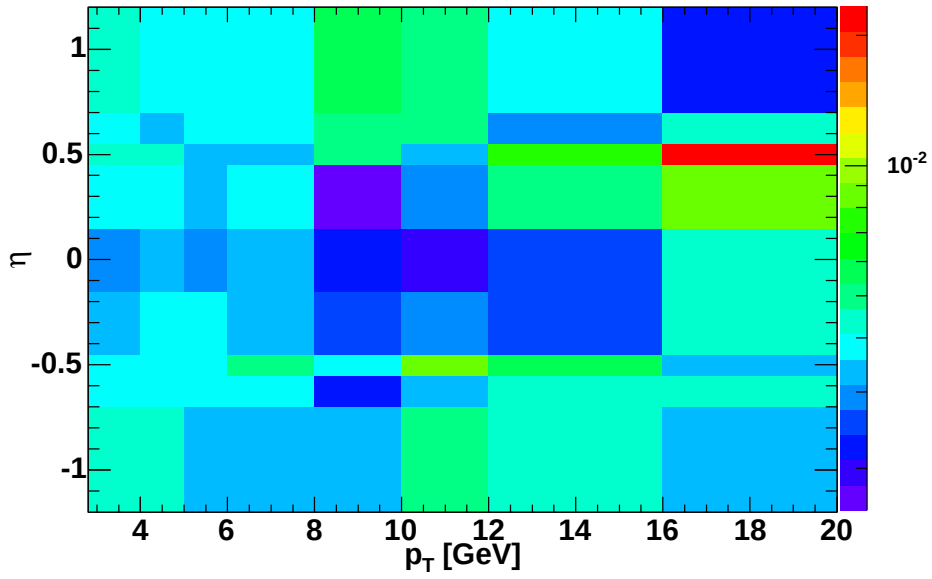

Figure 26: Fake rate matrix in bins of p_T and η using the W sample composition.

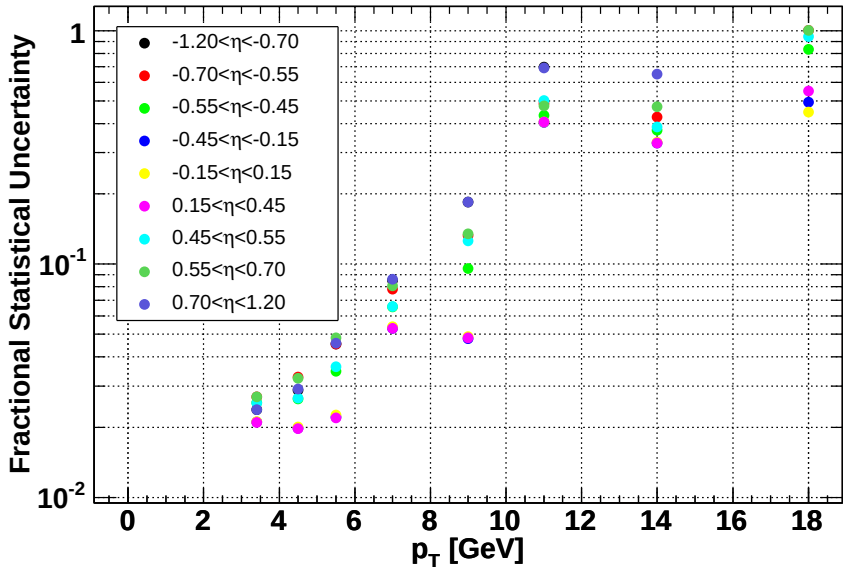

Figure 27: Fractional statistical ID rate uncertainty for the η and p_T bins used in the ID rate matrix.

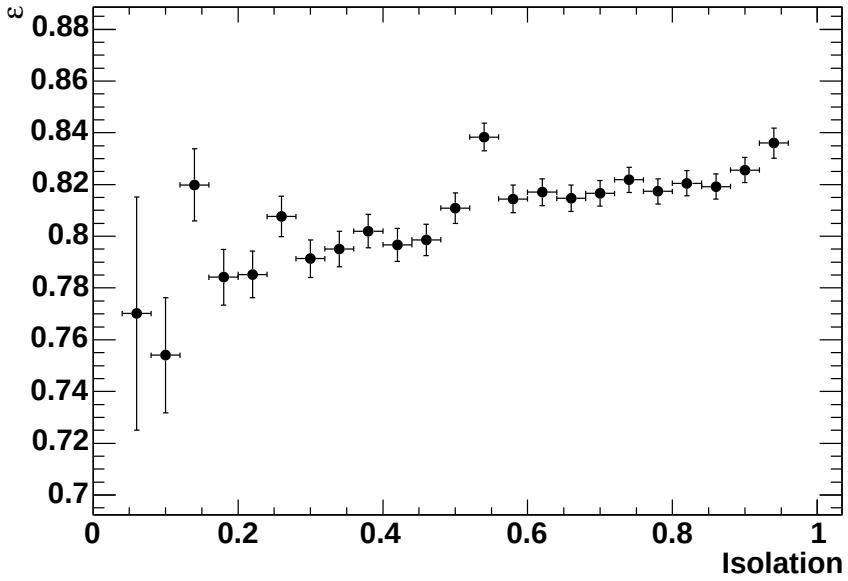

Figure 28: Soft muon identification efficiency as a function of the fractional isolation of the muon obtained from the J/ψ sample.

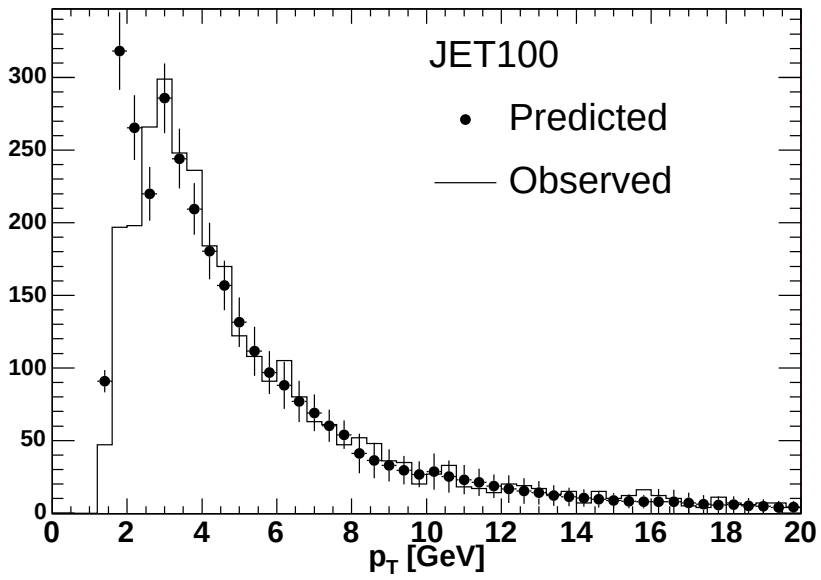

Figure 29: Observed and predicted soft muon rate in the JET50 sample with the selections as described in the text as a function of p_T.

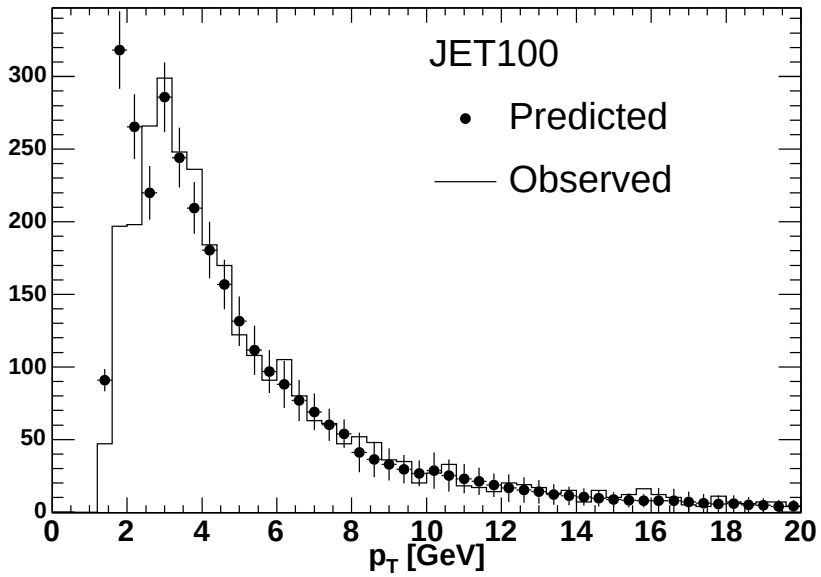

Figure 30: Observed and predicted soft muon rate in the JET100 sample with the selections as described in the text as a function of p_T.

8 Background Prediction

8.1 Heavy Flavor Fraction

Leptonic decays of heavy flavor is a significant background contribution to the soft leptons that we look for. In order to properly scale this background, we use the K-factor of 1.45 found in Ref. [22]. However, looking at the p_T^{rel} and σ_{d_0} distributions for the soft muons, we find that this does not sufficiently scale up the heavy flavor fraction in our sample. Therefore, we perform a simultaneous fit of p_T^{rel} and σ_{d_0} templates for heavy flavor, light flavor, and Drell-Yan processes to the data. (See Figure 31.) We use the scale factors found in this fit as a systematic.

8.2 Normalization of Soft Lepton Multiplicities

In the "Number of additional soft leptons" distributions, we normalize the MC to the number of data events found in the "exactly one additional lepton" bin. For bins which include additional electrons but no additional muons, we normalize to the "one additional electron" bin. For bins which include additional muons but no additional electrons, we normalize to the "one additional muon" bin. For bins which include additional electrons and muons, we normalize to the electrons and use the normalization to the muons as a systematic error.

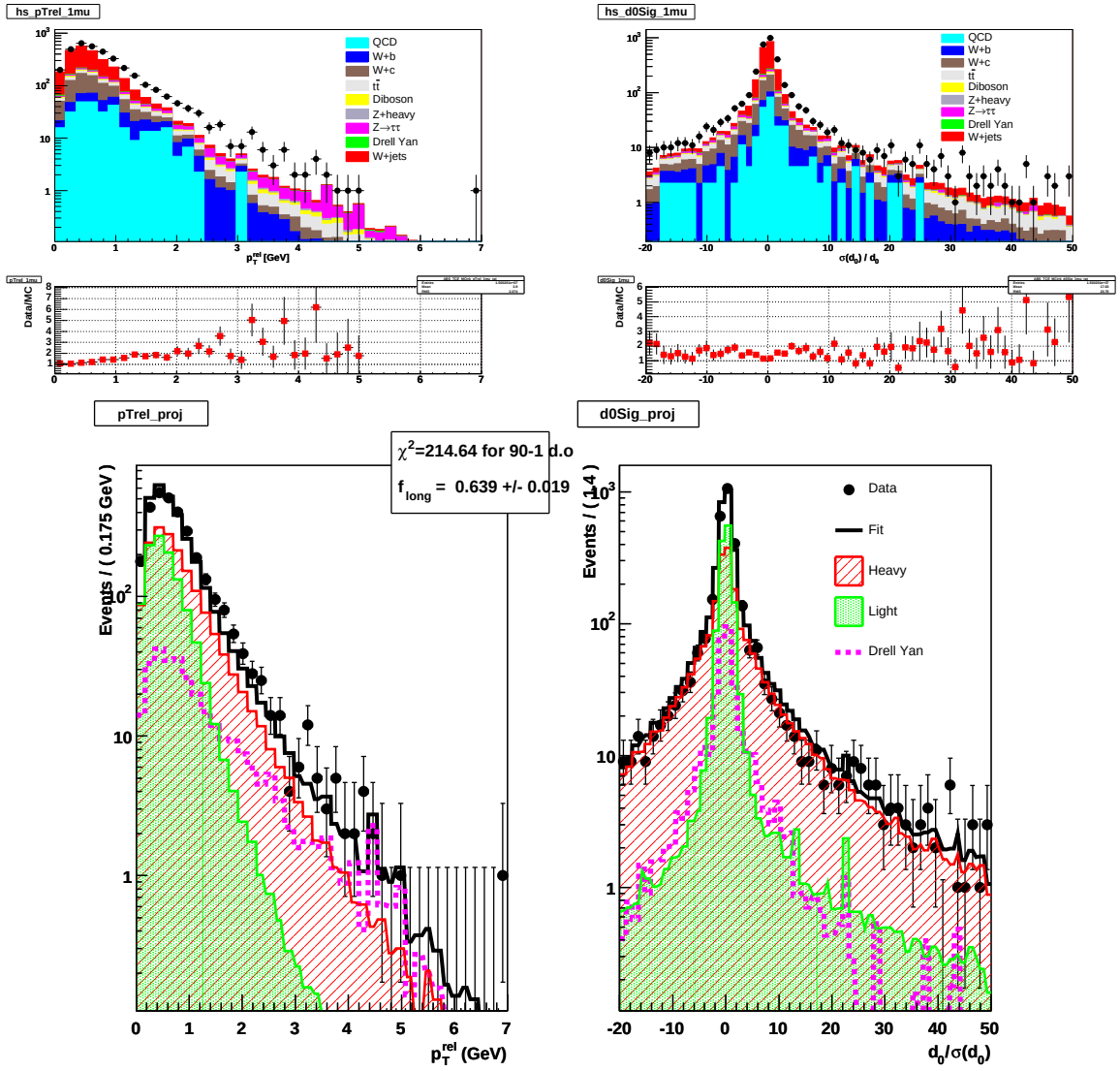

Figure 31: Plots showing the discrepancy in p_T^{rel} and σ_{d_0} before the heavy flavor fit (above) and the result of the simultaneous fit to p_T^{rel} and σd_0.

Systematic Source	Size	Effect in Large S/B Region
Trigger Efficiency (Sec. 6.3)	$\pm$(1.6 - 5.9)%	$\pm$0.06
QCD fraction (Sec. 5)	$\pm$26%	0
Soft e real rate (Sec. 7.1.3)	$\pm$15%	$\pm$0.04
Soft e fake rate (Sec. 7.1.3)	$\pm$15%	$\pm$0.11
Soft μ real rate (Sec. 7.2.3)	$\pm$ stat. err. in matrix $\pm$8%	$\pm$0.64
Soft μ fake rate (Sec. 7.2.3)	$\pm$10%	$\pm$0.34
Normalization to e or μ (Sec. 8.2)	$\pm$(48 - 62)%	$\pm$0.12
Heavy Flavor Fraction (Sec. 8.1)	+(84 - 225)%	$\pm$1.51

Table 16: Sources of systematic errors and their effects on the "$\geq$ 3 additional muons" region. Note that, although some of the systematics are very large, they have almost no effect in the signal region, due to there being very little SM background in this region.

9 Systematics

The sources of systematic errors are summarized in Table 16. They are more fully described in the sections listed in the table. Their effect is measured in a "Large S/B Region" where most of our limit-setting power comes from, defined as ≥ 3 additional muons. In this region, we expect 1.9 SM background events and 21.9 signal events.

10 Results

Figures 32 and 33 show the multiplicity of additional electrons and muons in W and Z events, with the Standard Model expectation and observed data overlaid. The two-dimensional histogram of N_μ vs. N_e is presented in slices of N_e for ease of viewing, and summarized in Table 17. As a reference, the expected signal distribution is shown from the "Neutralino Benchmark Model" described in Ref. [9], with parameters listed in Table 18.

Good agreement with the standard model expectation is observed across the distributions.

This model has a cross-section of 389 fb to produce W/Z + Higgs. We proceed to set a limit in the Bayesian framework of $0.069 \times \sigma$, or 27 fb, at 95% credibility. We can rule out the model at the standard cross section at a confidence level of 99.7% in the modified frequentist framework. Both of these limits are set using the MCLIMIT code[23].

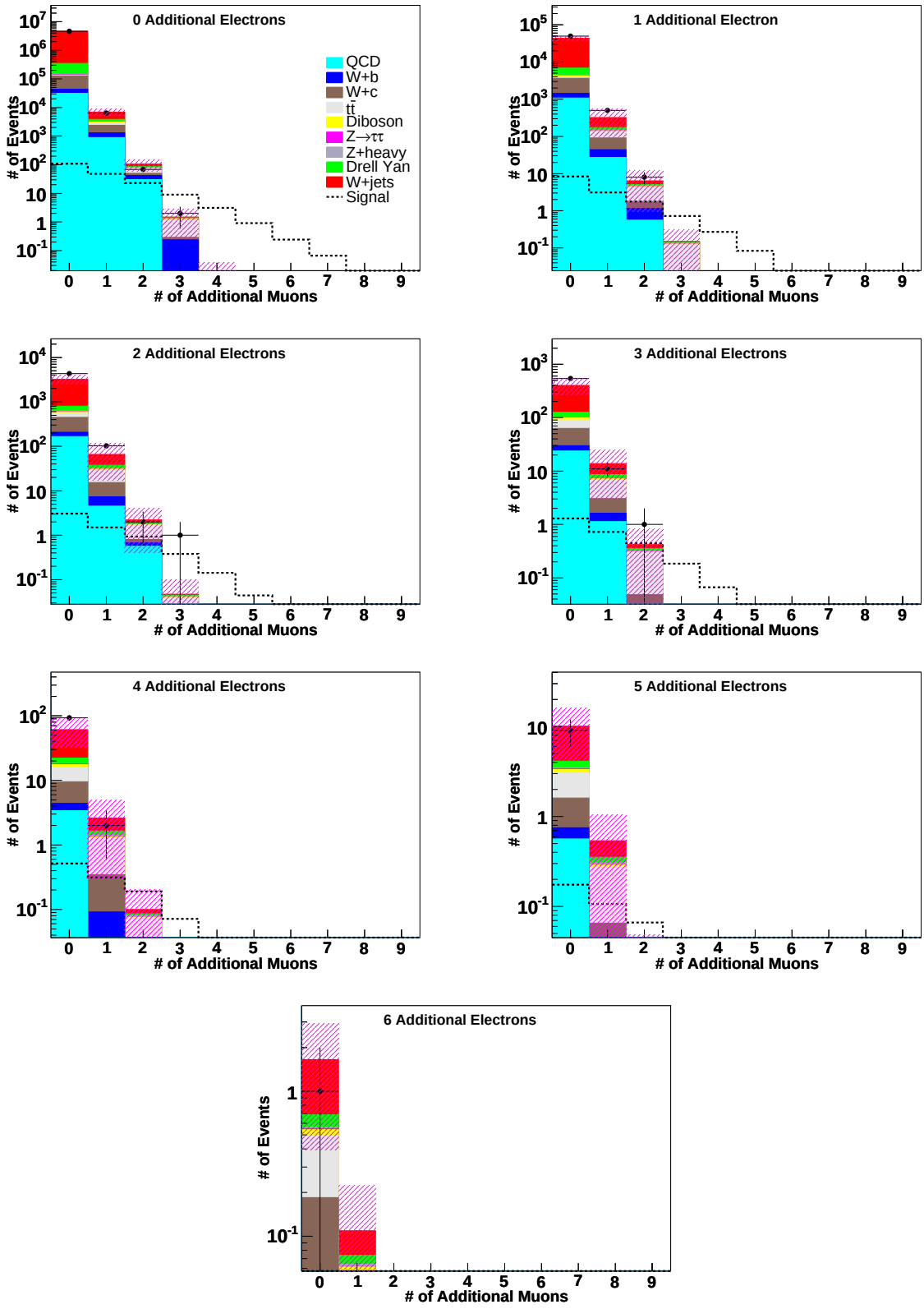

Figure 32: Muon multiplicity distribution for the W selection in bins of electron multiplicity. Both hard and soft leptons (but not the initial trigger lepton) are counted. Note that the plots combine the electron- and muon-triggered events.

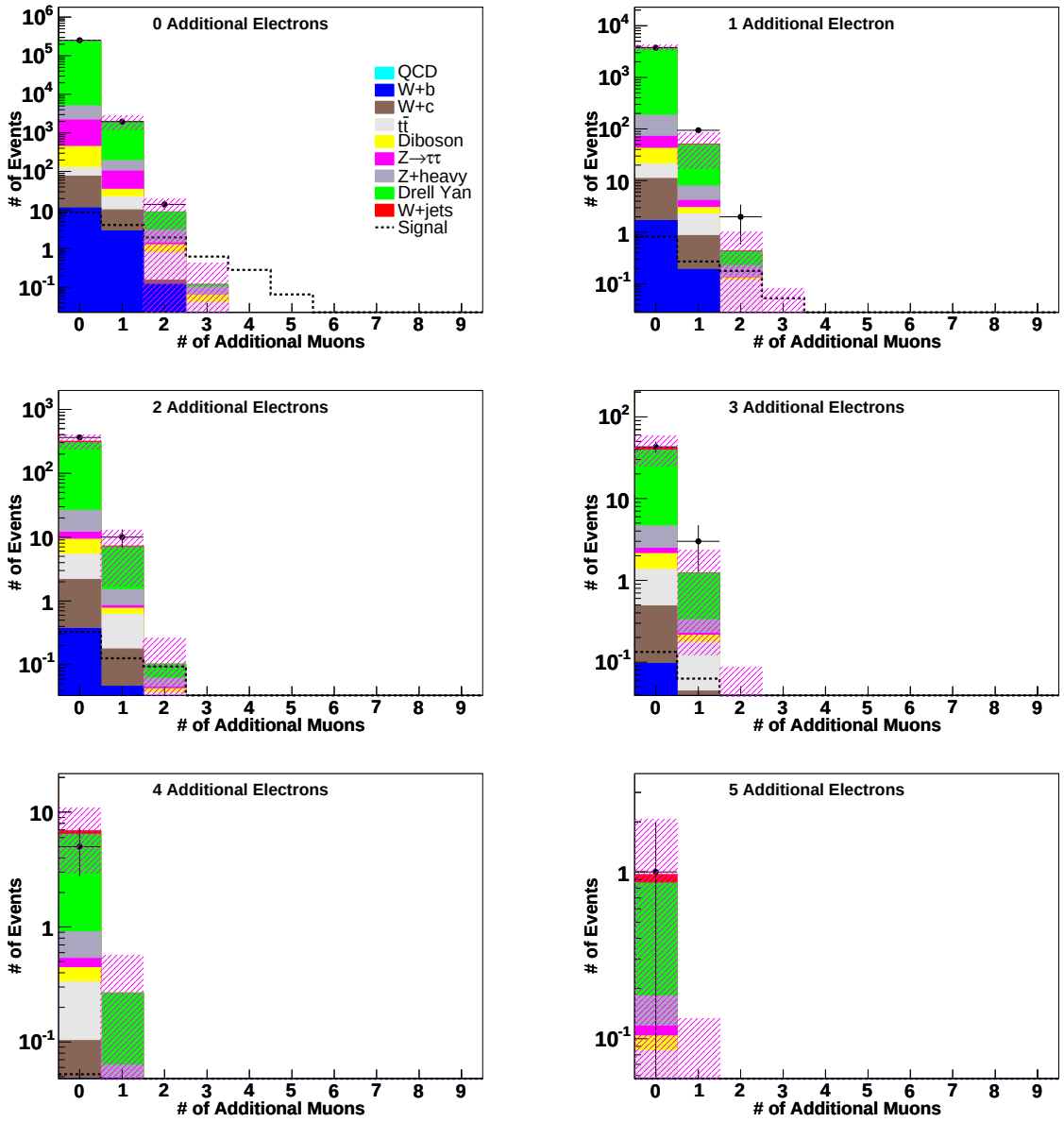

Figure 33: Muon multiplicity distribution for the Z selection in bins of electron multiplicity. Both hard and soft leptons (but not the initial trigger leptons) are counted. Note that the plots combine the electron- and muon-triggered events.

N_e	N_μ	Predicted SM Background	Predicted Dark Higgs Signal	Observed
0	0	4632580 ± 21334	108	4660910
0	1	6999 ± 1831	48	6402
0	2	106 ± 45	23	69
0	3	1.5 ± 1.2	9.0	2
0	4	0.019 ± 0.020	3.1	0
0	5	0.00018 ± 0.00021	0.92	0
1	0	43551 ± 5403	8.3	49420
1	1	323 ± 227	3.1	498
1	2	6.4 ± 5.5	1.8	8
1	3	0.15 ± 0.16	0.72	0
1	4	0.0025 ± 0.0031	0.27	0
2	0	3237 ± 763	3.1	4310
2	1	66 ± 49	1.5	103
2	2	2.2 ± 1.8	0.93	2
2	3	0.047 ± 0.051	0.38	1
3	0	402 ± 139	1.3	538
3	1	14 ± 11	0.72	11
3	2	0.42 ± 0.41	0.45	1
4	0	61 ± 28	0.51	93
4	1	2.6 ± 2.3	0.31	2
5	0	10 ± 6.0	0.17	9
5	1	0.54 ± 0.52	0.11	0

N_e	N_μ	Predicted SM Background	Predicted Dark Higgs Signal	Observed
0	0	244858 ± 3263	8.8	252132
0	1	1964 ± 783	4.1	1976
0	2	9.0 ± 11	2.0	14
0	3	0.12 ± 0.30	0.63	0
0	4	0 ± 0.00094	0.28	0
1	0	3797 ± 495	0.82	3747
1	1	51 ± 34	0.27	94
1	2	0.43 ± 0.61	0.18	2
2	0	318 ± 79	0.33	363
2	1	7.2 ± 5.5	0.13	10
3	0	42 ± 17	0.13	43
3	1	1.2 ± 1.1	0.063	3
4	0	6.9 ± 3.9	0.052	5
4	1	0.27 ± 0.30	0.019	0
5	0	0.97 ± 1.1	0.017	1

Table 17: Summary of predicted and observed event counts by number of additional electrons and muons after the W selection (top) and Z selection (bottom). Bins with less than 0.25 expected events in both signal and background and 0 observed events are not shown.

Parameter	Value
μ	149 GeV
m_1(bino)	13 GeV
m_2(wino)	286 GeV
$\tan(\beta)$	3.5
$\sin(\alpha)$	-0.28
m_{χ_0}	10 GeV
m_H	120 GeV
m_{χ_d}	1 GeV
m_{γ_d}	300 MeV
BR($\chi_0 \to \chi_d + 2\gamma_d$)	33%
BR($\chi_0 \to \chi_d + 3\gamma_d$)	33%
BR($\chi_0 \to \chi_d + 4\gamma_d$)	33%

Table 18: Parameters that we use for the benchmark model. The branching fractions for $\chi_0 \to \chi_d + N\gamma_d$ are a simple way to model the cascade decays through the hidden sector.

11 Conclusions

We have performed a broad search for additional electrons and muons with p_T above a low threshold (3 GeV for muons and 1 GeV for electrons) in W and Z events. The signature of multiple leptons is common in many models of new physics with light mass scales and couplings to the Electroweak sector, including NMSSM [2], little Higgs models [3], and R-parity violating MSSM models [4].

The results are presented in bins of the number of additional leptons in order to facilitate comparison with a wide range of models, present and future. We observe no excess over the predicted Standard Model background. We set a limit on a hidden-sector dark Higgs model as a representative of this class of models.

References

[1] R. Barate *et al.*, Phys. Lett. B.**565**, 61 (2003).

[2] R. Dermisek and J. F. Gunion, Phys. Rev. Lett. **95**, 041801 (2005); R. Dermisek and J. F. Gunion, Phys. Rev. D. **75**, 075019 (2007).

[3] B. Bellazzini, C. Csaki, A. Falkowski, and A. Weiler, Phys. Rev. D **80**, 075008 (2009).

[4] L. M. Carpenter, D. E. Kaplan and E. J. Rhee, Phys. Rev. Lett. **99**, 211801 (2007).

[5] M. J. Strassle and K. M. Zurek, Phys. Rev. Lett. B **651**, 374 (2007); T. Han, Z. Si, K. M. Zurek, and M. J. Strassler JHEP **0807**, 008 (2008).

[6] O. Adriania *et al.* [PAMELA Collaboration], Nature **458**, 607 (2009); F. Aharonian *et al.* [H.E.S.S Collaboration], Phys. Rev. Lett. **101**, 261104 (2008); A. A. Abdo *et al.* [Ferma LAT Collaboration], Phys. Rev. Lett. **102**, 181101 (2009).

[7] N. Arkani-Hamed, D. P. Finkbeiner, T. R. Slayter and N. Weiner, Phys. Rev. D **79**, 015014 (2009); P. Meade, M. Papucci, A. Strumia, and T. Volansky, arXiv:0905.0480 [hep-ph]; M. Pospelov and A. Ritz, Phys. Lett. B **671**, 391 (2009); I. Z. Rothstein, T. Schwetz and J. Zupan, JCAP **0907**, 018 (2009); C. Cheung, J. T. Ruderman, L. T. Wang and I. Yavin, Phys. Rev. D **80**, 035008 (2009); A. Katz and R. Sundrum, JHEP **0906**, 003 (2009).

[8] J. T. Ruderman and T. Volansky, arXiv:0908.1570 [hep-ph]; X. Chen, JCAP **0909**, 029 (2009); J. Mardon, Y. Normura and J. Thaler, Phys. Rev. D **80** 035013 (2009).

[9] A. Falkowski, J. T. Ruderman, T. Voalnsky and J. Zupan, JHEP **1005**, 077 (2010); A. Falkowski, J. T. Ruderman, T. Volansky and J. Zupan, Phys. Rev. Lett. **105**, 241801 (2010).

[10] M. L. Mangano, M. Moretti, F. Piccinini, R. Pittau, A. Polosa, "ALPGEN, a generator for hard multiparton processes in hadronic collisions", JHEP 0307:001 (2003)

[11] T. Sjostrand, S. Mrenna, P. Skands, "PYTHIA 6.4 Physics and Manual", JHEP 0605:026 (2006)

[12] http://www-cdf.fnal.gov/internal/physics/joint_physics/instructions/

[13] F. A. Berends, W. T. Giele, H. Kuijf, R. Kleiss, and W. James Striling, Phys. Lett. B **224**, (1989).

[14] S. Paramonov, "A Limit on the Branching Ratio of the Flavor-Changing Top Quark Decay t–¿Zc.", FERMILAB-THESIS-2009-12

[15] B. Cooper and A. Messina, "Estimation of the Background to $W^{\pm} \to e^{\pm}\nu + n$ Jet Events", CDF Note 6636.

[16] http://www-cdf.fnal.gov/tiki/tiki-index.php?page=Stntuple.Datasets.HighPtData

[17] CDF Collaboration, "Search for the Neutral Current Top Quark Decay $t \to Zc$ Using the Ratio of Z-Boson + 4 Jets to W-Boson + 4 Jets Production", Phys.Rev.D80:052001,2009

[18] V. Tiwari, G. Giurgiu, M. Paulini, J. Russ, "Likelihood Based Electron Tagging", CDF Note 7121

[19] S. Fidele and P. Murat, "2D Reconstruction of the CES Showers and Identification of High-P_t Electrons", CDF Note 7097

[20] L. Cerrito and A. Taffard, *"A Soft Muon Tagger For Run II: Summer-04 version"*, CDF Note 7122 (2004).

[21] A. Bridgeman, L. Cerrito, U. Grundler, T. Liss, and X. Zhang, *"A Heavy Flavor-Free Mistag Matrix for the Soft Muon Tagger"*, CDF Note 9083 (2008).

[22] A. Ivanov, T. Schwartz, R. Erbacher, "Calibration of Heavy-Flavor Content in W + Jets Data", CDF Note 9403

[23] T. Junk, NIM A434, p. 435-443 (1999)

A Monte Carlo Datasets

The Alpgen W + jets and W + heavy datasets are shown in Tables 19 and 20, and the Alpgen Drell-Yan and Drell-Yan + heavy datasets are shown in Tables 21 and 22. The Pythia datasets are shown in Table 23.

Process	σ	Dataset (low $\mathcal{L}$)	$N_{events}(low\ \mathcal{L})$	Dataset (high $\mathcal{L}$)	$N_{events}(high\ \mathcal{L})$
$W(e\nu) + 0p$	2.52 nb	pt0sw0	4929337	ut0s00	1985030
$W(e\nu) + 1p$	315 pb	pt0sw1	4909767	ut0s01	1984122
$W(e\nu) + 2p$	49.42 pb	pt0s2w	918835	ut0s02	400219
$W(e\nu) + 3p$	7.83 pb	pt0s3w	783415	ut0s03	396219
$W(e\nu) + \geq 4p$	1.44 pb	pt0s4w	453531	ut0s04	396219
$W(\mu\nu) + 0p$	2.52 nb	pt0sw5	5010637	ut0s05	1985030
$W(\mu\nu) + 1p$	315 pb	pt0sw6	4997783	ut0s06	1985030
$W(\mu\nu) + 2p$	49.42 pb	pt0s7w	877801	ut0s07	400219
$W(\mu\nu) + 3p$	7.83 pb	pt0s8w	817043	ut0s08	400219
$W(\mu\nu) + \geq 4p$	1.44 pb	pt0s9w	906265	ut0s09	400219
$W(\tau\nu) + 0p$	2.52 nb	ut0sw0	4868422	ut0s10	1984200
$W(\tau\nu) + 1p$	315 pb	ut0sw1	4981403	ut0s11	1985030
$W(\tau\nu) + 2p$	49.56 pb	ut0s2w	917094	ut0s12	400219
$W(\tau\nu) + 3p$	7.84 pb	ut0s3w	1008221	ut0s13	400219
$W(\tau\nu) + \geq 4p$	1.44 pb	ut0s4w	986494	ut0s14	396219

Table 19: Alpgen $W+$ partons dataset names, processes, cross sections, and number of events generated. Note that the cross-sections listed include a K-factor of 1.4.

Process	σ	Dataset (low $\mathcal{L}$)	$N_{events}(low\ \mathcal{L})$	Dataset (high $\mathcal{L}$)	$N_{events}(high\ \mathcal{L})$
$W(e\nu) + bb + 0p$	4.17 pb	bt0s0w	1541069	bt0s00	593755
$W(e\nu) + bb + 1p$	1.24 pb	bt0s1w	1545970	bt0s01	594426
$W(e\nu) + bb+ \geq 2p$	402 fb	bt0s2w	1498550	bt0s02	604337
$W(\mu\nu) + bb + 0p$	4.17 pb	bt0s5w	1539099	bt0s05	605333
$W(\mu\nu) + bb + 1p$	1.24 pb	bt0s6w	1529300	bt0s06	601125
$W(\mu\nu) + bb+ \geq 2p$	400 fb	bt0s7w	1501959	bt0s07	593788
$W(\tau\nu) + bb + 0p$	4.17 pb	dt0sw0	769285	bt0s10	601802
$W(\tau\nu) + bb + 1p$	1.24 pb	dt0sw1	1105495	bt0s11	596337
$W(\tau\nu) + bb+ \geq 2p$	400 fb	dt0sw2	1468622	bt0s12	592389
$W(e\nu) + cc + 0p$	7.00 pb	ct0s0w	2008023	bt0s15	796448
$W(e\nu) + cc + 1p$	2.51 pb	ct0s1w	1983960	bt0s16	772496
$W(e\nu) + cc+ \geq 2p$	879 fb	ct0s2w	2001927	bt0s17	777696
$W(\mu\nu) + cc + 0p$	7.00 pb	ct0s5w	2018429	bt0s21	800448
$W(\mu\nu) + cc + 1p$	2.51 pb	ct0s6w	2025229	bt0s22	792448
$W(\mu\nu) + cc+ \geq 2p$	879 fb	ct0s7w	1990504	bt0s23	788236
$W(\tau\nu) + cc + 0p$	7.00 pb	et0sw0	1973192	bt0s25	788448
$W(\tau\nu) + cc + 1p$	2.51 pb	et0sw1	1985097	bt0s26	796690
$W(\tau\nu) + cc+ \geq 2p$	879 fb	et0sw2	1921088	bt0s27	786908
$W(e\nu) + c + 0p$	23.9 pb	st0sw0	1960065	ot0swd	800448
$W(e\nu) + c + 1p$	4.75 pb	st0sw1	1964891	ot0swe	800448
$W(e\nu) + c + 2p$	710 fb	st0sw2	1978900	ot0swf	799773
$W(\mu\nu) + c + 0p$	23.9 pb	st0sw5	1992335	ot0swh	800448
$W(\mu\nu) + c + 1p$	4.75 pb	st0sw6	1984842	ot0swi	800448
$W(\mu\nu) + c + 2p$	710 fb	st0sw7	1974052	ot0swj	799678
$W(\tau\nu) + c + 0p$	23.9 pb	st0swa	1532572	ot0swl	800448
$W(\tau\nu) + c + 1p$	4.75 pb	st0swb	1532908	ot0swm	800448
$W(\tau\nu) + c + 2p$	710 fb	st0swc	1504501	ot0swn	800448
$W(\tau\nu) + c+ \geq 3p$	116 fb	st0swd	1510193	ot0swo	800448

Table 20: Alpgen $W+$ heavy dataset names, processes, cross sections, and number of events generated. Note that the cross-sections listed include a K-factor of 1.4.

Process	σ	Dataset (low $\mathcal{L}$)	$N(low\ \mathcal{L})$	Dataset (high $\mathcal{L}$)	$N(high\ \mathcal{L})$
$Z(ee) + 0p$ [75 : 105]	158 pb	zt0sp0	2639520	bt0sz0	880438
$Z(ee) + 1p$ [75 : 105]	21.6 pb	zt0sp1	2624793	bt0sz1	1024551
$Z(ee) + 2p$ [75 : 105]	3.46 pb	zt0szb	4595453	bt0sz2	1793000
$Z(ee) + 3p$ [75 : 105]	0.55 pb	zt0s3p	524261	bt0sz3	192119
$Z(ee) + \geq 4p$ [75 : 105]	99.2 fb	zt0s4p	525065	bt0sz4	192119
$Z(\mu\mu) + 0p$ [75 : 105]	158 pb	zt0sp5	2659832	bt0sz5	1020551
$Z(\mu\mu) + 1p$ [75 : 105]	21.6 pb	zt0sp6	2652428	bt0sz6	1021555
$Z(\mu\mu) + 2p$ [75 : 105]	3.46 pb	zt0szt	4660506	bt0sz7	1793000
$Z(\mu\mu) + 3p$ [75 : 105]	0.55 pb	zt0s8p	536159	bt0sz8	192119
$Z(\mu\mu) + \geq 4p$ [75 : 105]	99.2 fb	zt0s9p	530242	bt0sz9	192119
$Z(\tau\tau) + 0p$ [75 : 105]	158 pb	zt0st3	5860164	bt0sza	2400920
$Z(\tau\tau) + 1p$ [75 : 105]	21.5 pb	zt0st4	5722772	bt0szb	2400920
$Z(\tau\tau) + \geq 2p$ [75 : 105]	4.14 pb	zt0st2	2263107	bt0szc	953280
$DY(ee) + 0p$ [8 : 20]	1514 pb	zt0sl0	531063	-	-
$DY(ee) + 1p$ [8 : 20]	19.7 pb	zt0sl1	530980	-	-
$DY(ee) + 2p$ [8 : 20]	6.98 pb	zt0sl2	519852	-	-
$DY(ee) + 0p$ [20 : 75]	160 pb	xt0s0p	536159	zt0so6	192119
$DY(ee) + 1p$ [20 : 75]	8.39 pb	xt0s1p	530958	zt0so7	192119
$DY(ee) + 2p$ [20 : 75]	1.61 pb	xt0s2p	536159	zt0so9	1793000
$DY(ee) + 3p$ [20 : 75]	233 fb	xt0s3p	525670	zt0soa	192119
$DY(ee) + \geq 4p$ [20 : 75]	39.8 fb	xt0s4p	515638	zt0sob	192119
$DY(ee) + 0p$ [105 : 600]	4.07 pb	yt0s0p	519104	zt0sol	192119
$DY(ee) + 1p$ [105 : 600]	705 fb	yt0s1p	524895	zt0som	192119
$DY(ee) + 2p$ [105 : 600]	117 fb	yt0s2p	513214	zt0son	192119
$DY(ee) + 3p$ [105 : 600]	18.5 fb	yt0s3p	504749	zt0soo	192119
$DY(\mu\mu) + 0p$ [8 : 20]	1514 pb	zt0sm0	530855	-	-
$DY(\mu\mu) + 1p$ [8 : 20]	19.7 pb	zt0sm1	525713	-	-
$DY(\mu\mu) + 2p$ [8 : 20]	6.98 pb	zt0sm2	530561	-	-
$DY(\mu\mu) + 0p$ [20 : 75]	160 pb	xt0s5p	519237	zt0soc	192119
$DY(\mu\mu) + 1p$ [20 : 75]	8.4 pb	xt0s6p	530696	zt0sod	192119
$DY(\mu\mu) + 2p$ [20 : 75]	1.6 pb	xt0s7p	520703	zt0sof	1792478
$DY(\mu\mu) + 3p$ [20 : 75]	233 fb	xt0s8p	509424	zt0sog	192119
$DY(\mu\mu) + \geq 4p$ [20 : 75]	39.8 fb	xt0s9p	523932	zt0soh	192119
$DY(\mu\mu) + 0p$ [105 : 600]	4.07 pb	yt0s5p	530941	zt0soq	192119
$DY(\mu\mu) + 1p$ [105 : 600]	706 fb	yt0s6p	529581	zt0sor	192119
$DY(\mu\mu) + 2p$ [105 : 600]	117 fb	yt0s7p	531006	zt0sos	192119
$DY(\mu\mu) + 3p$ [105 : 600]	18.5 fb	yt0s8p	510246	zt0sot	192119
$DY(\tau\tau) + 0p$ [20 : 75]	160 pb	xt0st0	1135920	-	-
$DY(\tau\tau) + 1p$ [20 : 75]	8.38 pb	xt0st1	1158902	-	-
$DY(\tau\tau) + \geq 2p$ [20 : 75]	1.82 pb	xt0st2	2270345	-	-
$DY(\tau\tau) + 0p$ [105 : 600]	4.07 pb	zt0s0h	268428	-	-
$DY(\tau\tau) + 1p$ [105 : 600]	707 fb	zt0s1h	268428	-	-
$DY(\tau\tau) + \geq 2p$ [105 : 600]	117 fb	zt0s2h	268428	-	-

Table 21: Alpgen Drell-Yan + partons dataset names, processes, cross sections, and number of events generated. The mass range column refers to the generated mass range of the dilepton pair. Note that the cross-sections listed do not include a K-factor.

Process	σ	Dataset (low $\mathcal{L}$)	$N(low\ \mathcal{L})$	Dataset (high $\mathcal{L}$)	$N(high\ \mathcal{L})$
$Z(ee) + bb + 0p$ [75 : 105]	511 fb	zt0sb0		bt0szd	1544133
$Z(ee) + bb + 1p$ [75 : 105]	134 fb	zt0sb1	536159	bt0sze	192056
$Z(ee) + bb+ \geq 2p$ [75 : 105]	38.5 fb	zt0sb2	525955	bt0szf	192119
$Z(\mu\mu) + bb + 0p$ [75 : 105]	511 fb	zt0sb5	529635	bt0szg	109368
$Z(\mu\mu) + bb + 1p$ [75 : 105]	134 fb	zt0sb6	530793	bt0szh	87944
$Z(\mu\mu) + bb+ \geq 2p$ [75 : 105]	38.5 fb	zt0sb7	525695	bt0szi	192119
$Z(\tau\tau) + bb+ \geq 0p$ [75 : 105]	625 fb	zt0sc0	536159	bt0szj	608337
$Z(ee) + cc + 0p$ [75 : 105]	511 fb	zt0sc0	1544133	bt0szk	284167
$Z(ee) + cc + 1p$ [75 : 105]	134 fb	zt0sc1	690239	bt0szl	288167
$Z(ee) + cc+ \geq 2p$ [75 : 105]	38.5 fb	zt0sc2	663518	bt0szm	288167
$Z(\mu\mu) + cc + 0p$ [75 : 105]	511 fb	zt0sc5	671375	bt0szn	288167
$Z(\mu\mu) + cc + 1p$ [75 : 105]	134 fb	zt0sc6	663431	bt0szo	288167
$Z(\mu\mu) + cc+ \geq 2p$ [75 : 105]	38.5 fb	zt0sc7	648338	bt0szp	288167
$Z(\tau\tau) + cc+ \geq 0p$ [75 : 105]	625 fb	zt0sct	2056891	bt0szq	800448
$DY(ee) + bb + 0p$ [20 : 75]	293 fb	xt0sb0	529488	-	-
$DY(ee) + bb + 1p$ [20 : 75]	58.5 fb	xt0sb1	534522	-	-
$DY(ee) + bb+ \geq 2p$ [20 : 75]	15.9 fb	xt0sb2	529502	-	-
$DY(\mu\mu) + bb + 0p$ [20 : 75]	293 fb	xt0sb5	529304	-	-
$DY(\mu\mu) + bb + 1p$ [20 : 75]	58.5 fb	xt0sb6	367279	-	-
$DY(\mu\mu) + bb+ \geq 2p$ [20 : 75]	15.8 fb	xt0sb7	528903	-	-
$DY(\tau\tau) + bb+ \geq 0p$ [20 : 75]	313 fb	xt0sbt	1510091	-	-
$DY(ee) + bb + 0p$ [105 : 600]	14.4 fb	yt0s0b	513872	-	-
$DY(ee) + bb + 1p$ [105 : 600]	4.2 fb	yt0s1b	529304	-	-
$DY(ee) + bb+ \geq 2p$ [105 : 600]	1.2 fb	yt0s2b	523926	-	-
$DY(\mu\mu) + bb + 0p$ [105 : 600]	14.4 fb	yt0s5b	534522	-	-
$DY(\mu\mu) + bb + 1p$ [105 : 600]	4.2 fb	yt0s6b	529385	-	-
$DY(\mu\mu) + bb+ \geq 2p$ [105 : 600]	1.2 fb	yt0s7b	529458	-	-
$DY(\tau\tau) + bb+ \geq 0p$ [105 : 600]	18.1 fb	yt0stb	1515347	-	-

Table 22: Alpgen Drell-Yan + heavy dataset names, processes, cross sections, and number of events generated. The mass range column refers to the generated mass range of the dilepton pair. Note that the cross-sections listed do not include a K-factor.

Dataset	Process	σ	N_{events}
tt0s75	$t\bar{t}$	7.0 pb	4730477
it0sww	Diboson (WW)	12.4 pb	2291309
it0swz	Diboson (WZ)	3.65 pb	2328823
it0szz	Diboson (ZZ)	3.8 pb	2319470

Table 23: Pythia dataset names, processes, cross sections, and number of events generated. The cross-sections listed include a K-factor of 1.40.